Composite Structures 284 (2022) 115083

Contents lists available at ScienceDirect

Composite Structures

journal homepage: www.elsevier.com/locate/compstruct

Static and dynamic NURBS-based isogeometric analysis of composite plates under hygrothermal environment

Abha Gupta [a,*,1], Surendra Verma [b,2], Anup Ghosh [b,3]

[a] Department of Aerospace Engineering, Punjab Engineering College (DU), Chandigarh 160012, India
[b] Department of Aerospace Engineering, IIT Kharagpur, West Bengal 721302, India

ARTICLE INFO

Keywords:
Isogeometric analysis
Hygrothermal analysis
Green–Lagrange nonlinearity
Fast Fourier transformation (FFT)
Multi-patch technique

ABSTRACT

In this paper, a computationally efficient isogeometric plate model, employing nonpolynomial shear deformation theory (NPSDT), for static and dynamic analysis of laminated and sandwich composite plates under hygrothermal environment is presented. Transient and steady-state response using Rayleigh damping model and fast Fourier transformation of transient response have also been obtained for the hygrothermal environment. The non-uniform rational B-splines (NURBS) based formulation has been considered, which attribute only five-degree of freedom and satisfies the stringent continuity requirement of the NPSDT model (C^1-continuity) without any additional variables. A total Lagrangian approach in conjunction with Hamilton's principle is utilized to formulate the governing equations for thermal bending and subsequent dynamic analysis of multilayered composite plates. To model stress stiffening effect due to hygrothermal load, both von Kármán and Green–Lagrange strain displacement relations are incorporated and obtained solutions are compared. It has been shown that at higher temperature (around one fourth of the critical buckling temperature), the consideration of Green–Lagrange strain relationship for modeling stiffening effect due to hygrothermal load is important for better accuracy. Further, it has been shown that bending strip is essential in case of higher-order shear deformation theory (HSDT) to get more accurate solution. In addition, the obtained transient damped/undamped solutions may be used to get the natural frequency from their FFT solution.

1. Introduction

Today's requirement for the highly effective and efficient material, concerned with the eco-friendly world of finite resources, has made the advanced composites to be one of the most important materials for the structural engineering. In the past few decades, laminated and sandwich composite structures achieved comprehensive recognition in industries like aerospace, mechanical, automotive, marine, etc. This is generally because of its excellent mechanical properties such as high stiffness-to-weight ratio, high strength-to-weight ratio, high impact, fatigue and corrosion resistance, and their easy tailoring capability to design any shape over the isotropic materials. However, the influence of transverse shear deformation is crucial in composites, due to their low shear to extensional modulus ratio, and cannot be ignored even for thin plate. Thus, structural analysis must consider the effect of shear deformation to fully utilize the performance of multilayered composite structures for wide range of applications. As a result, several approximate plate theories have been developed by various researchers to evaluate the structural responses of multilayered composite structures under static and dynamic loads. For instance, first-order shear deformation theory (FSDT), which includes constant transverse shear deformation with only C° continuity of generalized displacement, became popular [1] in compare to classical laminated plate theory (CLPT) which completely ignores transverse shear effects. Further, a shear correction factor has been introduced to adjust the transverse shear energy of FSDT. However, the accuracy is difficult to ascertain due to dependency of the shear correction factor on the lamination sequence, loading conditions, and boundary conditions [2,3]. Later on, these limitations of FSDT have been overcome by the introduction of higher-order shear deformation theories (HSDTs). In general, transverse shear deformations are modeled using HSDT which either considers the displacement field of higher-order terms from Taylor's series expansion, called polynomial shear deformation theories (PSDTs) [4], or utilizes nonpolynomial function in the

* Corresponding author.
E-mail addresses: abhagupta@pec.edu.in (A. Gupta), surendraverma2501@gmail.com (S. Verma), anup@aero.iitkgp.ac.in (A. Ghosh).
[1] Assistant Professor, PEC Chandigarh.
[2] Research Scholar, IIT Kharagpur.
[3] Associate Professor, IIT Kharagpur.

https://doi.org/10.1016/j.compstruct.2021.115083
Received 6 August 2021; Received in revised form 30 November 2021; Accepted 4 December 2021
Available online 7 January 2022

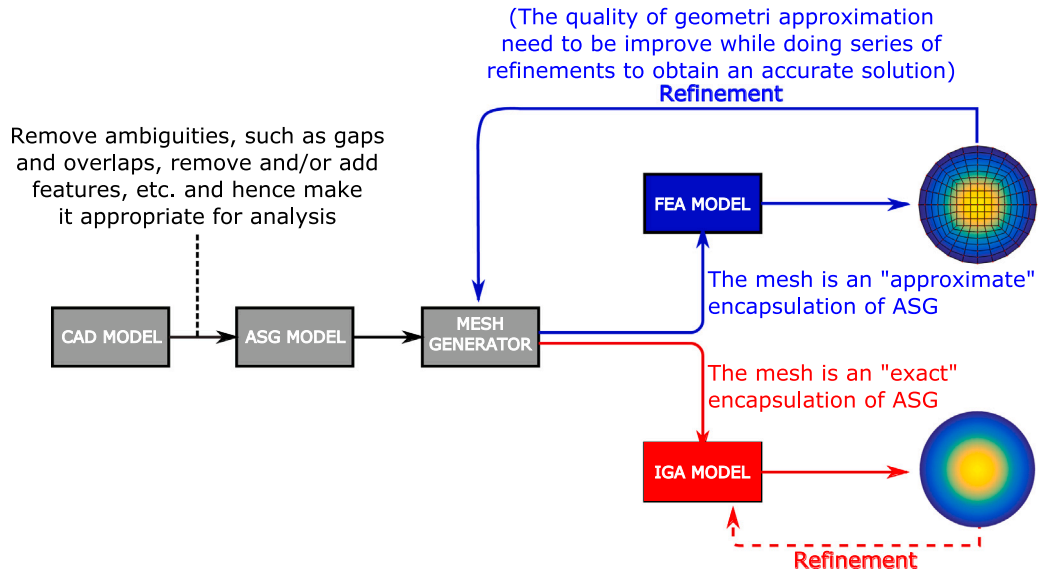

Fig. 1. Steps involved from CAD designing to analysis procedures.

displacement field, called nonpolynomial shear deformation theories (NPSDTs) [5–7]. Among various researchers, Reddy [4] has done noticeable work in the development of HSDT and detailed work on PSDT and NPSDT can be found in review papers [1,5]. Shear strain function in NPSDT can be of different kinds [1] such as inverse hyperbolic, inverse trigonometric, algebraic, exponential, logarithmic, trigonometric, and/or their combined functions. It is emphasized in the literature that the NPSDT provides significantly large scope to increase the modeling accuracy [1,8]. Hence, due to this advantageous properties, NPSDT has been considered for the present structural analysis.

In structural analysis, first CAD (Computer Aided Design) files are generated by the designers and then these are translated into analysis-suitable geometries (ASG), meshed and given as a input to the CAE (Computer Aided Engineering) for the numerical analysis. The numerical approach used in CAE is in general the finite element analysis (FEA) which most commonly utilizes C^0 Lagrange basis function to approximate the unknown field variables; while different basis functions are used in CAD model. Thus, the mesh in finite element method (FEM) is an approximate encapsulation of ASG, which in turn leads to a disconnection between FEA and CAD design, and attributes to the origin of many practical issues arising in CAE. Moreover, the construction of finite element mesh, including the approximation of CAD model and mesh refinement, can be quite time-consuming [9]. Additionally, the use of different basis functions made the communication between CAD and CAE time-consuming and laborious [10] as illustrated in Fig. 1.

Substantial efforts have been made to obviate these shortcomings by Hughes et al. [9,11] through integrating CAD and CAE within an isogeometric analysis (IGA) framework. The usage of same geometric language in CAD and analysis is the fundamental of IGA [11] which makes it an improvised technique than the FEM. The IGA aims to integrate the design with analysis using the same basis function, which helps to eliminate the need for communication with the CAD geometry [11–14] (see Fig. 1).

In general, the structures are exposed to changing environmental conditions during their service life; during this, temperature and moisture have an adverse effect on the performance of these structures [15]. Also, during the manufacturing of composite material, heating and cooling processes are followed with variation in the range of 200 °C to 300 °C for polymer matrix composite [16]. This heating and cooling induce thermal stresses in the composite material due to mismatch of the thermal coefficients of the fiber and matrix. Likewise, the polymer matrix also has the capability of absorption and desorption of moisture, which leads to swelling strains and stresses. Further, the effective residual stresses in the laminae are different in each ply due to the different alignment of fiber in each lamina. Thus, knowing the prevailing impact of elevated temperature and moisture concentration on the characteristics of composite material, which are vastly used in an aerospace application, it is essential to investigate the structural response of composite plate subjected to the hygrothermal environment during the design and analysis process for better reliability and maintenance of these structures [17].

Several researchers have worked on the static analysis of composite plate under hygrothermal environment utilizing polynomial shear deformation theory [16,18,19]. Apart from this, few have also studied the static analysis using nonpolynomial shear deformation theory like Zenkour [20] and Joshan et al. [21]. Further, several recent work on thermo-mechanical analysis of multilayered plates have been carried out by Moleiro et al. [22], Han et al. [23] and Murugesan et al. [24]. For exhaustive literature on static analysis of laminated and sandwich composite plate under hygrothermal load, a recent review article by Garg and Chalak [16] can also be referred. However, all these works are primarily confined to the cross-ply laminated composite plates. Moreover, the effect of transformation matrix for the thermal coefficient has not been comparatively studied in the literature. Also, the comprehensive effects of temperature-dependent and temperature-independent material properties are not assessed in the available literature. Therefore, in the present work, these aspects are being taken care for the static analysis of laminated composite plate under hygrothermal environment.

Further, the effect of hygrothermal environment on the dynamic characteristics of composite plate has also been studied by several researchers [25–29]. However, all these works are limited to the CLPT and FSDT which have their own limitations in regards to the accuracy. Therefore, some researchers have worked with higher-order theories which takes into account the discrepancies of FSDT. Like, Makhecha et al. [30] employed higher-order quasi-3D theory to study the influence of thickness stretching for linear transient analysis of laminated composite plate under thermal loading. Then, Matsunaga [31] proposed a global higher-order deformation theory to determine the linear natural frequency and critical buckling temperature of an angle-ply laminated and sandwich composite plates under thermal environment. Recently, Zenkour and Bouazza [32] analytically examined the free vibration characteristics of multilayered composite plate under hygrothermal environment by the means of refined hyperbolic shear deformation theory. Further, Vinyas and Kattimani [33] assessed the free vibration characteristic of magneto-electro-elastic rectangular

plates in hygrothermal environment using TSDT under finite element framework. More recently, Thakur et al. [15] have studied the dynamic response of composite plate under hygrothermal environment utilizing a higher-order nonpolynomial shear deformation theory.

It is evident from above literature that the FEM has been exhaustively used for the static and dynamic analysis under hygrothermal environment; however, most of them deal with the cross-ply laminate with the consideration of von Kármán nonlinearity to model thermal induced stresses. Apart from finite element method, researchers have also studied the structural response of multilayered composite plate using isogeometric analysis, however, without considering hygrothermal environment [34–37]. Further, multi-patch technique with/without bending strip plays an important role in isogeometric analysis and few researchers [38–42] have studied this without considering hygrothermal environment. Moreover, as per author's knowledge, in the viewpoint of isogeometric analysis, very few studies have been reported on static and dynamic analysis of multilayered composite plate under hygrothermal environment. For instance, Tran et al. [43] utilized a third-order shear and normal deformation theory to investigate the thermal bending and buckling response of laminated composite plate. Recently, Gupta and Ghosh [44] analyzed the thermo-elastic bending behavior of the laminated composite plate using FSDT by the means of isogeometric method. Further, Phung-Van et al. [45,46] proposed an IGA approach for the nonlinear analysis of functionally graded material plated. Moreover, for the analysis of functionally graded microplates based on the modified couple stress theory, Nguyen et al. [47] proposed a quasi-3D isogeometric approach. Cuong-Le et al. [48] utilized the IGA approach for the 3D analysis of free vibration and buckling of annular plate, conical, cylindrical shell of FG porous-cellular materials.

Through the concise literature review presented above, it has been shown that there is a scarcity in the literature related to NURBS-based structural analysis of multilayered composite plates under hygrothermal environment. Only few papers are available which incorporates PSDT for the hygrothermal analysis. Moreover, stress stiffening effect incorporating Green–Lagrange is not considered in the literature even with FSDT, TSDT or collectively PSDT. As per authors' knowledge, despite the development of various NPSDTs [5,49], rarely any literature has been reported on static and dynamic analysis of laminated and sandwich composite plate using IGA under hygrothermal environment utilizing NPSDT. Also, the damped transient analysis of laminated composite plate under hygrothermal environment has not been discussed adequately. Moreover, the utilization of multi-patch and bending strip, and their importance for the analysis of free vibration under hygrothermal environment has not been discussed properly in the literature. Further, the use of fast Fourier transform (FFT) and harmonic analysis to study the frequency response has rarely been observed in the literature.

Therefore, in this paper, an attempt has been made to fulfill these gaps with novel solutions and discussions. Here, the characteristic of NURBS-based IGA plays an advantageous role in assessing stress stiffening effect in the initial stress matrix by providing C^1 inter-element continuity and leads to five degrees of freedom (DOFs) only, instead of seven DOFs in C° finite element method. Also, a comparative study is carried out between von Kármán and Green–Lagrange stress stiffening effect in the dynamic analysis. The critical temperature has also been studied to provide a safeguard for the structural design. Rayleigh damping model is employed to study damped transient and steady state response. Finally, the accuracy of the proposed IGA-NPSDT plate model is verified by comparing the present solutions with available analytical and numerical solutions, as well as with the present obtained Navier and 3D elasticity solutions. Further, an extensive parametric study has been carried out by presenting several relevant numerical examples.

1.1. Contributions of the present work

- As per author's knowledge, for the first time, extensive static and dynamic response under hygrothermal environment for IGA-NPSDT model is presented.
- A detailed discussion and the repercussion of multi-patch with/without bending strip is elucidated.
- The accuracy benefit and utilization condition of Green–Lagrange over von Kármán for modeling stiffening effect of hygrothermal load is illustrated.
- The FFT solution of damped/undamped transient response and harmonic solution for various thermal load.
- Evaluation of accuracy of various polynomial and nonpolynomial shear deformation theory for isogeometric analysis under hygrothermal load.

2. Isogeometric analysis

2.1. NURBS

Non-uniform rational B-splines (NURBS), a superset of B-spline, possesses the inherent quality to precisely represent the complex geometry such as circles, spheres, etc., which cannot be done by B-splines. Representation of such geometries using NURBS can be achieved by the piecewise projective transformation of the B-splines curve, which leads to rational basis functions. B-spline curves in $\mathbb{R}^d$ Euclidean space are constructed by taking a linear combination of B-spline basis functions with control points. The more detail about the B-spline curve has been discussed in the other paper of the author [10] and the same notations have been considered here as well.

2.1.1. NURBS curves and surface

A NURBS entity in $\mathbb{R}^d$ Euclidean space is obtained by projecting a B-spline entity in $\mathbb{R}^{d+1}$, where d is the number of physical dimensions. NURBS basis functions are evaluated by augmenting every control point, P_A, in control mesh with the homogeneous coordinate w_A, which are scalar in nature, also known as weights. The NURBS surface is then defined by

$$S(\xi,\eta) = \frac{\sum_{A=1}^{n\times m} N_A^b(\xi,\eta) w_A P_A}{\sum_{A=1}^{n\times m} N_A^b(\xi,\eta)\, w_A} = \sum_{A=1}^{n\times m} R_A(\xi,\eta)\, P_A \tag{1}$$

where, $R_A(\xi,\eta) = N_A^b(\xi,\eta) w_A / \left(\sum_{A=1}^{n\times m} N_A^b(\xi,\eta)\, w_A\right)$ is the 2D NURBS basis function.

The choice of the weight in the NURBS basis function depends on the CAD model considered for the analysis [50] and which can be calculated using Eq. (1). For rectangular geometry, B-spline basis functions are sufficient to represent the geometry accurately by considering $w_A = 1$ [50], which is a special case of NURBS basis functions.

The B-spline (or NURBS) can be enriched by three types of refinements — knot insertion, degree elevation (or order elevation), and degree and continuity elevation. The first two are equivalent to h- and p-refinement, respectively, while the last one is k-refinement that does not exist in standard FEM [11].

3. Mathematical formulation

In this section, mathematical formulation for static and dynamic analysis of multilayered composite plate is described. The structural behavior is assumed to be uncoupled with heat transfer and moisture absorption process.

The problem starts with the input of steady state temperature, T or moisture, C profile over the plate. Further, the effect of hygrothermal

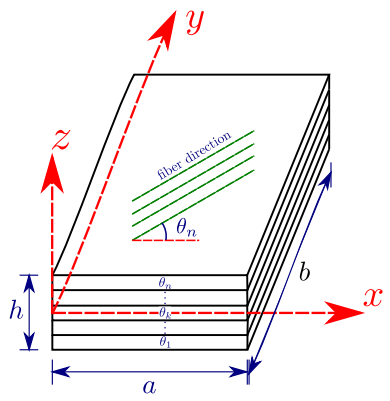

Fig. 2. Schematic diagram of a multilayered composite plate.

environment in present formulation is incorporated using induced non-mechanical strain. The total strain under hygrothermal effect is equal to the summation of mechanical strains and non-mechanical hygrothermal strains. The non-mechanical induced strains incorporate the change in temperature, $\Delta T = T - T_{\text{ref}}$ and change in moisture, $\Delta C = C - C_{\text{ref}}$ from their reference paradigm, T_{ref} and C_{ref}. But, here, the formulation is restricted to thermal effect only as similar procedure may be followed for the moisture-induced strain with standard $C_{\text{ref}} = 0\%$.

To demonstrate the formulation, a rectangular multilayered composite plate with side length, a, width, b and uniform thickness, h is considered. The composite plate is composed of n orthotropic ply stacked in particular orientation as shown in Fig. 2 with $x - y - z$ Cartesian coordinate system.

3.1. Displacement field model

Based on the equivalent higher-order shear deformation theory (HSDT), the assumed displacement field can be defined in unified form as follows:

$$\begin{aligned} u(x,y,z,t) &= u_0(x,y,t) - z\frac{\partial w_0}{\partial x} + f(z)\theta_x(x,y,t) \\ v(x,y,z,t) &= v_0(x,y,t) - z\frac{\partial w_0}{\partial y} + f(z)\theta_y(x,y,t) \\ w(x,y,z,t) &= w_0(x,y,t) \end{aligned} \tag{2}$$

where u, v and w are the displacement of the arbitrary point along the Cartesian axis x, y and z, respectively. The quantities u_0, v_0, w_0, θ_x and θ_y are five degrees of freedom at the arbitrary point located on midplane of the plate. The function $f(z)$ incorporate the nonlinearity in the transverse strain and physically represents the warping of the cross-section perpendicular to mid-plane. This equivalent displacement model can be reduced to FSDT and CLPT models by considering $f(z) = z$ [51] with shear correction factor in the transverse shear energy and $f(z) = 0$, respectively. The third-order shear deformation theory, which is a polynomial based higher-order theory, can be obtained by taking $f(z) = z - 4z^3/3h^2$ [52]. In our present study, two nonpolynomial shear deformation theories are utilized which are given as follows: (a) Inverse hyperbolic shear deformation theory (IHSDT) [21], $f(z) = sinh^{-1}(3z/h) - 6z/h\sqrt{13}$ and (b) Inverse hyperbolic tangent shear deformation theory (IHTSDT) [53], $f(z) = tanh^{-1}(0.088z/h) - 0.088(z/h)/(1 - 0.088^2/4)$.

3.2. Strain–displacement relation

In orthonormal Cartesian coordinate system, the state-of-strain, $\boldsymbol{\varepsilon}$ at a point, using Green–Lagrange strain relation, is expressed as

$$\boldsymbol{\varepsilon} = \begin{Bmatrix} \frac{\partial u}{\partial x} \\ \frac{\partial v}{\partial y} \\ \frac{\partial u}{\partial y} + \frac{\partial v}{\partial x} \\ \frac{\partial v}{\partial z} + \frac{\partial w}{\partial y} \\ \frac{\partial u}{\partial z} + \frac{\partial w}{\partial x} \end{Bmatrix} + \frac{1}{2}\begin{Bmatrix} \left(\frac{\partial u}{\partial x}\right)^2 + \left(\frac{\partial v}{\partial x}\right)^2 + \left(\frac{\partial w}{\partial x}\right)^2 \\ \left(\frac{\partial u}{\partial y}\right)^2 + \left(\frac{\partial v}{\partial y}\right)^2 + \left(\frac{\partial w}{\partial y}\right)^2 \\ 2\left(\frac{\partial u}{\partial x}\frac{\partial u}{\partial y} + \frac{\partial v}{\partial x}\frac{\partial v}{\partial y} + \frac{\partial w}{\partial x}\frac{\partial w}{\partial y}\right) \\ 2\left(\frac{\partial u}{\partial y}\frac{\partial u}{\partial z} + \frac{\partial v}{\partial y}\frac{\partial v}{\partial z} + \frac{\partial w}{\partial y}\frac{\partial w}{\partial z}\right) \\ 2\left(\frac{\partial u}{\partial x}\frac{\partial u}{\partial z} + \frac{\partial v}{\partial x}\frac{\partial v}{\partial z} + \frac{\partial w}{\partial x}\frac{\partial w}{\partial z}\right) \end{Bmatrix} = \boldsymbol{\varepsilon}_l + \frac{1}{2}\boldsymbol{\varepsilon}_{nl} \tag{3}$$

For present displacement model, given in Eq. (2), linear strain vector, $\boldsymbol{\varepsilon}_l$ can be separated into inplane strain vector, $\boldsymbol{\varepsilon}_{lb} = \left\{\frac{\partial u}{\partial x}, \frac{\partial v}{\partial y}, \frac{\partial u}{\partial y} + \frac{\partial v}{\partial x}\right\}$ and transverse strain vector, $\boldsymbol{\varepsilon}_{ls} = \left\{\frac{\partial v}{\partial z} + \frac{\partial w}{\partial y}, \frac{\partial u}{\partial z} + \frac{\partial w}{\partial x}\right\}$ as

$$\boldsymbol{\varepsilon}_l = \begin{Bmatrix} \boldsymbol{\varepsilon}_{lb} \\ \boldsymbol{\varepsilon}_{ls} \end{Bmatrix} = \begin{Bmatrix} \boldsymbol{Z}_{lb}\hat{\boldsymbol{\varepsilon}}_{lb} \\ \boldsymbol{Z}_{ls}\hat{\boldsymbol{\varepsilon}}_{ls} \end{Bmatrix} \tag{4}$$

in which (see Eqs. (5a) and (5b) are given as in Box I)

Similarly, after substituting the expression of the HSDT from Eq. (2), nonlinear strain vector, $\boldsymbol{\varepsilon}_{nl}$ can be rewritten as

$$\boldsymbol{\varepsilon}_{nl} = \begin{Bmatrix} \boldsymbol{\varepsilon}_{nlb} \\ \boldsymbol{\varepsilon}_{nls} \end{Bmatrix} = \begin{Bmatrix} \boldsymbol{Z}_{nlb}\boldsymbol{A}_b\boldsymbol{\phi}_b \\ \boldsymbol{Z}_{nls}\boldsymbol{A}_s\boldsymbol{\phi}_s \end{Bmatrix} = \begin{Bmatrix} \boldsymbol{Z}_{nlb}\hat{\boldsymbol{\varepsilon}}_{nlb} \\ \boldsymbol{Z}_{nls}\hat{\boldsymbol{\varepsilon}}_{nls} \end{Bmatrix} \tag{6}$$

in which $\boldsymbol{Z}_{nlb}$ and $\boldsymbol{Z}_{nls}$ are the matrix of thickness component, while $\hat{\boldsymbol{\varepsilon}}_{nlb}$ and $\hat{\boldsymbol{\varepsilon}}_{nls}$ represent the generalized nonlinear strain vector. The explicit expression of these matrices and vectors are given as (see Eqs. (7a)–(7d) are given as in Boxes II, III, IV and V)

3.3. Constitutive relation

The constitutive relation for an arbitrary k^{th} orthotropic layer with zero normal stress condition, in Cartesian coordinate system, (x, y, z) including thermal effect, is given by Duhamel–Neumann's law as

$$\boldsymbol{\sigma}_m^{(k)} = \left[\mathscr{T}_{trans}^{(k)}\right]\boldsymbol{Q}^{(k)}\left[\mathscr{T}_{trans}^{(k)}\right]^T\left(\boldsymbol{\varepsilon}^{(k)} - \boldsymbol{\varepsilon}_{\Delta T}^{(k)}\right) = \bar{\boldsymbol{Q}}^{(k)}\boldsymbol{\varepsilon}^{(k)} - \bar{\boldsymbol{Q}}^{(k)}\boldsymbol{\varepsilon}_{\Delta T}^{(k)} = \boldsymbol{\sigma}^{(k)} - \boldsymbol{\sigma}_{\Delta T}^{(k)} \tag{8}$$

where, $\boldsymbol{\sigma}$, $\boldsymbol{\sigma}_m$, $\boldsymbol{\sigma}_{\Delta T}$, $\boldsymbol{\varepsilon}$, $\boldsymbol{\varepsilon}_{\Delta T}$, and $\bar{\boldsymbol{Q}}$ are (total) stress, mechanical stress, thermal stress, (total) strain, thermal strain vector, and material constant matrix, respectively. The explicit relation and details of transformation matrix, $\left[\mathscr{T}_{trans}\right]$, material constant matrix, $\bar{\boldsymbol{Q}}$, and thermal strain vector, $\boldsymbol{\varepsilon}_{\Delta T}^{(k)}$ can be found in Ref. [10] or any standard book on laminated composite [54].

Consequently, the in-plane stress resultants and transverse shear resultants are defined using $\{\boldsymbol{\sigma}_m\} = \left\{\sigma_{xx_m}, \sigma_{yy_m}, \tau_{xy_m}, \tau_{yz_m}, \tau_{xz_m}\right\}^T$ as follows-

$$\begin{bmatrix} N_{xx} & M_{xx} & P_{xx} & Q_{xx} & R_{xx} & S_{xx} \\ N_{yy} & M_{yy} & P_{yy} & Q_{yy} & R_{yy} & S_{yy} \\ N_{xy} & M_{xy} & P_{xy} & Q_{xy} & R_{xy} & S_{xy} \end{bmatrix} = \int_{-h/2}^{h/2}\begin{Bmatrix} \sigma_{xx_m} \\ \sigma_{yy_m} \\ \tau_{xy_m} \end{Bmatrix}\left\{1 \quad z \quad f(z) \quad z^2 \quad zf(z) \quad f^2(z)\right\}dz \tag{9}$$

$$\begin{bmatrix} N_{yz} & M_{yz} & P_{yz} & Q_{yz} & R_{yz} & S_{yz} \\ N_{xz} & M_{xz} & P_{xz} & Q_{xz} & R_{xz} & S_{xz} \end{bmatrix} = \int_{-h/2}^{h/2}\begin{Bmatrix} \tau_{yz_m} \\ \tau_{xz_m} \end{Bmatrix}\left\{1 \quad z \quad f(z) \quad f'(z) \quad zf'(z) \quad f(z)f'(z)\right\}dz$$

$$\hat{\boldsymbol{\varepsilon}}_{lb} = \left\{ \frac{\partial u_0}{\partial x} \quad \frac{\partial v_0}{\partial y} \quad \frac{\partial u_0}{\partial y} + \frac{\partial v_0}{\partial x} \quad -\frac{\partial^2 w_0}{\partial x^2} \quad -\frac{\partial^2 w_0}{\partial y^2} \quad -2\frac{\partial^2 w_0}{\partial x \partial y} \quad \frac{\partial \theta_x}{\partial x} \quad \frac{\partial \theta_y}{\partial y} \quad \frac{\partial \theta_x}{\partial y} + \frac{\partial \theta_y}{\partial x} \right\}^T \tag{5a}$$

$$\hat{\boldsymbol{\varepsilon}}_{ls} = \left\{ \theta_y \quad \theta_x \right\}^T ; \boldsymbol{Z}_{lb} = \begin{bmatrix} 1 & 0 & 0 & z & 0 & 0 & f(z) & 0 & 0 \\ 0 & 1 & 0 & 0 & z & 0 & 0 & f(z) & 0 \\ 0 & 0 & 1 & 0 & 0 & z & 0 & 0 & f(z) \end{bmatrix}; \boldsymbol{Z}_{ls} = \begin{bmatrix} f'(z) & 0 \\ 0 & f'(z) \end{bmatrix} \tag{5b}$$

Box I.

$$\boldsymbol{Z}_{nlb} = \begin{bmatrix} 1 & 0 & 0 & z & 0 & 0 & f(z) & 0 & 0 & z^2 & 0 & 0 & zf(z) & 0 & 0 & (f(z))^2 & 0 & 0 \\ 0 & 1 & 0 & 0 & z & 0 & 0 & f(z) & 0 & 0 & z^2 & 0 & 0 & zf(z) & 0 & 0 & (f(z))^2 & 0 \\ 0 & 0 & 1 & 0 & 0 & z & 0 & 0 & f(z) & 0 & 0 & z^2 & 0 & 0 & zf(z) & 0 & 0 & (f(z))^2 \end{bmatrix} \tag{7a}$$

Box II.

$$\boldsymbol{Z}_{nls} = \begin{bmatrix} 1 & 0 & z & 0 & f(z) & 0 & f'(z) & 0 & zf'(z) & 0 & f(z)f'(z) & 0 \\ 0 & 1 & 0 & z & 0 & f(z) & 0 & f'(z) & 0 & zf'(z) & 0 & f(z)f'(z) \end{bmatrix} \tag{7b}$$

Box III.

$$\boldsymbol{\phi}_b = \left\{ \frac{\partial u_0}{\partial x} \quad \frac{\partial u_0}{\partial y} \quad \frac{\partial v_0}{\partial x} \quad \frac{\partial v_0}{\partial y} \quad \frac{\partial w_0}{\partial x} \quad \frac{\partial w_0}{\partial y} \quad \frac{\partial^2 w_0}{\partial x^2} \quad \frac{\partial^2 w_0}{\partial x \partial y} \quad \frac{\partial^2 w_0}{\partial y \partial x} \quad \frac{\partial^2 w_0}{\partial y^2} \quad \frac{\partial \theta_x}{\partial x} \quad \frac{\partial \theta_x}{\partial y} \quad \frac{\partial \theta_y}{\partial x} \quad \frac{\partial \theta_y}{\partial y} \right\}^T \tag{7c}$$

Box IV.

$$\boldsymbol{\phi}_s = \left\{ \frac{\partial w_0}{\partial x} \quad \frac{\partial w_0}{\partial y} \quad \theta_x \quad \theta_y \quad \frac{\partial u_0}{\partial x} \quad \frac{\partial u_0}{\partial y} \quad \frac{\partial v_0}{\partial x} \quad \frac{\partial v_0}{\partial y} \quad \frac{\partial^2 w_0}{\partial x^2} \quad \frac{\partial^2 w_0}{\partial x \partial y} \quad \frac{\partial^2 w_0}{\partial y \partial x} \quad \frac{\partial^2 w_0}{\partial y^2} \quad \frac{\partial \theta_x}{\partial x} \quad \frac{\partial \theta_x}{\partial y} \quad \frac{\partial \theta_y}{\partial x} \quad \frac{\partial \theta_y}{\partial y} \right\}^T \tag{7d}$$

Box V.

3.4. Equations of motion

For arbitrary space variable and admissible virtual displacement $\delta\{u, v, w\}$, Hamilton's principle of the given system using total Lagrangian formulation [55] is written as

$$\delta \int_{t_i}^{t_f} \mathscr{L} dt = \int_{t_i}^{t_f} \left(\delta\mathscr{K} - \delta\mathscr{U} + \delta\mathscr{W}_{ext} \right) dt = 0 \tag{10}$$

Herein, all the kinematic and stress variables are expressed with reference to the undeformed configuration at time $t = 0$ s.

The first term in the Eq. (10) represents the virtual kinetic energy and is expressed as

$$\delta\mathscr{K} = -\int_V \rho\, \delta\boldsymbol{u}^T\, \ddot{\boldsymbol{u}}\, dz\, d\Omega \tag{11}$$

where, ρ is the mass density per unit volume, and $\boldsymbol{u}$ is the displacement vector. By following Eq. (2), displacement vector, $\boldsymbol{u}$ can be written in matrix form as $\boldsymbol{u} = \boldsymbol{Z}\,\bar{\boldsymbol{u}}$ mentioned in Ref. [10]. Using this, the virtual kinetic energy can be rewritten as

$$\delta\mathscr{K} = -\int_\Omega \delta\bar{\boldsymbol{u}}^T \boldsymbol{m}\, \ddot{\bar{\boldsymbol{u}}}\, d\Omega; \quad \boldsymbol{m} = \int_{-h/2}^{h/2} \rho\, \boldsymbol{Z}^T\, \boldsymbol{Z}\, dz \tag{12}$$

The second term in the Eq. (10) represents the virtual strain energy and is expressed as

$$\begin{aligned} \delta\mathscr{U} &= \int_V \left(\delta\boldsymbol{\epsilon} - \delta\boldsymbol{\epsilon}_{\Delta T} \right)^T \boldsymbol{\sigma}_m\, dz d\Omega = \int_V \delta\boldsymbol{\epsilon}^T \boldsymbol{\sigma}_m\, dz d\Omega \\ \delta\mathscr{U}_1 - \delta\mathscr{U}_2 &= \int_V \delta\boldsymbol{\epsilon}^T \left(\boldsymbol{\sigma} - \boldsymbol{\sigma}_{\Delta T} \right) dz d\Omega = \int_V \left(\delta\boldsymbol{\epsilon}_l + \delta\boldsymbol{\epsilon}_{nl} \right)^T \boldsymbol{\sigma}\, dz d\Omega \\ &\quad - \int_V \left(\delta\boldsymbol{\epsilon}_l + \delta\boldsymbol{\epsilon}_{nl} \right)^T \boldsymbol{\sigma}_{\Delta T} \end{aligned} \tag{13}$$

The last term of the Eq. (10) represents the virtual work done by transverse mechanical loading and is expressed as

$$\delta\mathscr{W}_{ext} = \int_\Omega \delta w_0 P(x, y, t)\, d\Omega \tag{14}$$

where, $P(x, y, t)$ is the time dependent distributed transverse load.

Now for the problem of interest in this study, i.e., dynamic analysis of plate structure in thermal environment, total Lagrangian approach is considered. To employ this, total solution is assumed as the sum of static solution, $\boldsymbol{u}^p$ due to change in temperature, and dynamic solution, $\boldsymbol{u}^d$ due to subsequent time dependent mechanical load, i.e., $\boldsymbol{u} = \boldsymbol{u}^p + \boldsymbol{u}^d$. Similarly, total strain, $\boldsymbol{\epsilon}$ can be split into static, $\boldsymbol{\epsilon}^p$ and dynamic, $\boldsymbol{\epsilon}^d$ part by following Eq. (3) with their corresponding mechanical stress part $\boldsymbol{\sigma}^p$ and $\boldsymbol{\sigma}^d$ as

$$\boldsymbol{\sigma}^p = \bar{\boldsymbol{Q}}\boldsymbol{\epsilon}^p \qquad \boldsymbol{\epsilon}^p = \boldsymbol{\epsilon}_l^p(\boldsymbol{u}^p) + \frac{1}{2}\boldsymbol{\epsilon}_{nl}^p(\boldsymbol{u}^p)$$

$$\boldsymbol{\varepsilon}^d = \boldsymbol{\varepsilon}_l^d(\boldsymbol{u}^d) + \frac{1}{2}\boldsymbol{\varepsilon}_{nl}^d(\boldsymbol{u}^d) + \boldsymbol{\varepsilon}_{nl}^p(\boldsymbol{u}^d) \quad (15a)$$

$$\boldsymbol{\sigma}^d = \bar{\boldsymbol{Q}}\boldsymbol{\varepsilon}^d \qquad \delta\boldsymbol{\varepsilon}^p = \delta\boldsymbol{\varepsilon}_l^p(\boldsymbol{u}^p) + \delta\boldsymbol{\varepsilon}_{nl}^p(\boldsymbol{u}^p)$$

$$\delta\boldsymbol{\varepsilon}^d = \delta\boldsymbol{\varepsilon}_l^d(\boldsymbol{u}^d) + \delta\boldsymbol{\varepsilon}_{nl}^d(\boldsymbol{u}^d) + \delta\boldsymbol{\varepsilon}_{nl}^p(\boldsymbol{u}^d) \quad (15b)$$

$$\boldsymbol{\varepsilon}_l^k(\boldsymbol{u}^*) = \boldsymbol{Z}_l\hat{\boldsymbol{\varepsilon}}_l(\boldsymbol{u}^*) \qquad \boldsymbol{\varepsilon}_{nl}^k(\boldsymbol{u}^*) = \boldsymbol{Z}_{nl}\boldsymbol{A}(\boldsymbol{u}^k)\boldsymbol{\phi}(\boldsymbol{u}^*)$$

$$\delta\boldsymbol{\varepsilon}_{nl}^k(\boldsymbol{u}^*) = \boldsymbol{Z}_{nl}\boldsymbol{A}(\boldsymbol{u}^k)\delta\boldsymbol{\phi}(\boldsymbol{u}^*) \quad (15c)$$

3.4.1. Bending analysis due to change in temperature

In the first stage of analysis, plate in undeformed (or reference) configuration is subjected to temperature change, ΔT. Thus Eq. (13) for admissible static displacement, $\delta\boldsymbol{u}^p$ can be rewritten as

$$\delta\mathscr{U} = \delta\mathscr{U}_1 - \delta\mathscr{U}_2 = \int_V \left(\delta\boldsymbol{\varepsilon}_l^p + \delta\boldsymbol{\varepsilon}_{nl}^p\right)^T \boldsymbol{\sigma}_p dz d\Omega - \int_V \left(\delta\boldsymbol{\varepsilon}_l^p + \delta\boldsymbol{\varepsilon}_{nl}^p\right)^T \boldsymbol{\sigma}_{\Delta T} = 0 \quad (16)$$

As present study is confined to geometrically linear analysis, $\delta\boldsymbol{\varepsilon}_{nl}^p = 0$; $\boldsymbol{\sigma}^p = \bar{\boldsymbol{Q}}\boldsymbol{\varepsilon}_l^p$ during the thermal load or environment (within the region of critical buckling temperature). Thus, Eq. (10) for static analysis due to temperature change becomes

$$\delta\mathscr{U} = \delta\mathscr{U}_1 - \delta\mathscr{U}_2 = \int_V \left(\delta\boldsymbol{\varepsilon}_l^p\right)^T \bar{\boldsymbol{Q}}\boldsymbol{\varepsilon}_l^p dz d\Omega - \int_V \left(\delta\boldsymbol{\varepsilon}_l^p\right)^T \boldsymbol{\sigma}_{\Delta T} = 0 \quad (17)$$

3.4.2. Dynamic analysis under thermal environment

In the second stage of analysis, total displacement, $\boldsymbol{u}(x,y,t) = \boldsymbol{u}^p(x,y) + \boldsymbol{u}^d(x,y,t)$ is considered with respect to undeformed (or reference) configuration with admissible dynamic displacement, $\delta\boldsymbol{u}^d$, $\delta\boldsymbol{\varepsilon}^d$, and $\delta\boldsymbol{\sigma}^d$. For this, expression for virtual kinetic energy, from Eq. (12) and strain energy, from Eq. (13) are obtained as

$$\delta\mathscr{K} = -\int_\Omega \left(\delta\ddot{\boldsymbol{u}}^d\right)^T \boldsymbol{m}\ddot{\boldsymbol{u}}^d d\Omega \quad (18)$$

$$\delta\mathscr{U} = \int_V \left(\delta\boldsymbol{\varepsilon}_l^d(\boldsymbol{u}_d) + \delta\boldsymbol{\varepsilon}_{nl}^p(\boldsymbol{u}_d) + \delta\boldsymbol{\varepsilon}_{nl}^d(\boldsymbol{u}_d)\right)^T \times \left(\boldsymbol{\sigma}^p(\boldsymbol{u}^p) + \boldsymbol{\sigma}^d(\boldsymbol{u}^d) - \boldsymbol{\sigma}_{\Delta T}\right) dz d\Omega \quad (19)$$

The virtual work done due to time dependent mechanical load after attaining the static equilibrium is obtained as

$$\mathscr{W}_{ext} = \int_\Omega \left(\delta w_{0s} + \delta w_{0d}\right) P(x,y,t)\, d\Omega = \int_\Omega \delta w_{0d} P(x,y,t)\, d\Omega \quad (20)$$

The assumption taken here is that the static displacement is not significant in compare to undeformed configuration of the plate, i.e., $\delta\boldsymbol{\varepsilon}_{nl}^p(\boldsymbol{u}^d) = 0$. Subsequently, a linear response is assumed due to the dynamic loading, i.e., $\boldsymbol{\sigma}^d = \bar{\boldsymbol{Q}}\boldsymbol{\varepsilon}_l^d(\boldsymbol{u}^d)$. After considering the above assumption and utilizing Eq. (17), virtual strain energy Eq. (19) for subsequent dynamic analysis of initially stressed plate is simplified to

$$\begin{aligned}\delta\mathscr{U} &= \int_V \left(\delta\left\{\boldsymbol{\varepsilon}_l^d(\boldsymbol{u}^d)\right\}^T \boldsymbol{\sigma}^d(\boldsymbol{u}^d)\right) dz d\Omega \\ &+ \int_V \left(\delta\left\{\boldsymbol{\varepsilon}_{nl}^d(\boldsymbol{u}^d)\right\}^T \boldsymbol{\sigma}^p(\boldsymbol{u}^p)\right) dz d\Omega \\ &= \int_V \left(\delta\left\{\boldsymbol{\varepsilon}_l^d(\boldsymbol{u}^d)\right\}^T \bar{\boldsymbol{Q}}\boldsymbol{\varepsilon}_l^d(\boldsymbol{u}^d)\right) dz d\Omega \\ &+ \int_V \left(\delta\left\{\boldsymbol{\phi}(\boldsymbol{u}^d)\right\}^T \mathbb{N}(\boldsymbol{u}^p)\left\{\boldsymbol{\phi}(\boldsymbol{u}^d)\right\}\right) d\Omega\end{aligned} \quad (21)$$

3.5. NURBS based discretization

The displacement field variables are interpolated using NURBS basis functions which can be written as

$$\boldsymbol{u} = \sum_{I=1}^{(p+1)\times(q+1)} [I_5] R_I \mathbf{q}_I \quad (22)$$

where, $(p+1)\times(q+1)$ is the number of basis functions, and $R_I(\xi,\eta)$, and $\mathbf{q}_I = \{u_{0I}\ v_{0I}\ w_{0I}\ \theta_{xI}\ \theta_{yI}\}^T$ are the NURBS basis functions and the degrees of freedom associated with control point I, respectively. In above equation, $[I_5]$ denotes the identity matrix.

Due to uncoupled nature of orthotropic material, strain energy can split into bending and transverse shear part. As a result, by substituting Eq. (22) into Eqs. (5), and (7), the generalized strain vector, $\hat{\boldsymbol{\varepsilon}}$ can be rewritten in terms of elemental strain–displacement matrix, $\boldsymbol{B}$ and elemental displacement vector, $\boldsymbol{q}$, for $(p, q) = 2$, as

$$\hat{\boldsymbol{\varepsilon}}_{li} = \sum_{I=1}^{9} \boldsymbol{B}_{iI}^L \boldsymbol{q}_I = \boldsymbol{B}_i^L \boldsymbol{q};\quad \hat{\boldsymbol{\varepsilon}}_{nli} = \sum_{I=1}^{9} \boldsymbol{A}_i \boldsymbol{G}_{iI}^{NL} \boldsymbol{q}_I = \sum_{I=1}^{9} \boldsymbol{B}_{iI}^{NL} \boldsymbol{q}_I = \boldsymbol{B}_i^{NL} \boldsymbol{q}$$

$$\boldsymbol{q} = \left\{u_{01}\ \ v_{01}\ \ w_{01}\ \ \theta_{x1}\ \ \theta_{y1}\ \ \cdots\ \ u_{09}\ \ v_{09}\ \ w_{09}\ \ \theta_{x9}\ \ \theta_{y9}\right\}^T \quad (23)$$

where, i = 'b' for bending and 's' for shear part.

The explicit expression of $\boldsymbol{B}_i^L$ and $\boldsymbol{G}_i^{NL}$ can obtained in terms of Cartesian derivatives of NURBS basis function. While using chain-rule, the first and second derivatives of NURBS basis functions (in Cartesian coordinate), used in strain–displacement matrix, can be calculated in terms of derivatives with respect to parametric coordinate [56, p. 99–100]. Finally, the parametric derivative of NURBS basis function can be obtained in terms of B-spline basis functions and further details regarding this can be found in [10,11].

3.6. System of equations

For static analysis, using Eqs. (17), (22) and (23) in Eq. (10), and by eliminating the virtual displacement vector, $\delta\boldsymbol{q}^p$, the system of equilibrium equations is obtained as

$$\boldsymbol{K}_l \boldsymbol{q}^p = \boldsymbol{F}_{\Delta T} \quad (24)$$

in which

$$\boldsymbol{K}_l = \int_\Omega \left(\boldsymbol{B}_b^{L^T} \boldsymbol{D}_{lbl} \boldsymbol{B}_b^L + \boldsymbol{B}_s^{L^T} \boldsymbol{D}_{lsl} \boldsymbol{B}_s^L\right) d\Omega;\quad \boldsymbol{F}_{\Delta T} = \int_\Omega \boldsymbol{B}^{L^T} \boldsymbol{Z}_l^T \boldsymbol{\sigma}_{\Delta T} d\Omega$$

$$\boldsymbol{D}_{lbl} = \int_{-h/2}^{h/2} \boldsymbol{Z}_{lb}^T \bar{\boldsymbol{Q}}_b \boldsymbol{Z}_{lb} dz;\quad \boldsymbol{D}_{lsl} = \int_{-h/2}^{h/2} \boldsymbol{Z}_{ls}^T \bar{\boldsymbol{Q}}_s \boldsymbol{Z}_{ls} dz$$

Similarly, using Eqs. (18) and (20) to (23) in Eq. (10), and eliminating the virtual displacement vector, $\delta\boldsymbol{q}^d$, the system of equations of motion in matrix form is obtained as

$$\boldsymbol{M}\ddot{\boldsymbol{q}}^d + \left(\boldsymbol{K}_l + \boldsymbol{K}_g(\boldsymbol{q}^p)\right)\boldsymbol{q}^d = \boldsymbol{F}_m \quad (25)$$

where, $\boldsymbol{K}_g(\boldsymbol{q}^p)$ represents the geometric stiffness matrix due to initial/static displacement, $\boldsymbol{q}^p$ obtained from Eq. (24), while $\boldsymbol{M}$, $\boldsymbol{F}_m$ and $\boldsymbol{q}^d$ represent mass matrix, time dependent mechanical force vector and subsequent dynamic displacement, respectively. Here, the incorporation of thermal effect has to be taken in the definition of stress resultants by following Eq. (8). The explicit relation of the geometric stiffness matrix is given as

$$\begin{aligned}\boldsymbol{K}_g &= \int_\Omega \left(\boldsymbol{B}^{NL^T}(\boldsymbol{q}^d)\boldsymbol{Z}_{nl}\boldsymbol{\sigma}(\boldsymbol{q}^p)\right) d\Omega \\ &= \int_\Omega \left(\boldsymbol{G}^{NL^T}\boldsymbol{A}(\boldsymbol{q}^d)\boldsymbol{Z}_{nl}\boldsymbol{\sigma}(\boldsymbol{q}^p)\right) d\Omega \\ &= \int_\Omega \left(\boldsymbol{G}^{NL^T}\mathbb{N}(\boldsymbol{q}^p)\boldsymbol{G}^{NL^T}\right) d\Omega \\ &= \left(\boldsymbol{G}_b^{NL^T}\mathbb{N}_b(\boldsymbol{q}^p)\boldsymbol{G}_b^{NL^T} + \boldsymbol{G}_s^{NL^T}\mathbb{N}_s(\boldsymbol{q}^p)\boldsymbol{G}_s^{NL^T}\right) d\Omega\end{aligned}$$

where, the expressions of $\mathbb{N}_b$ and $\mathbb{N}_s$ are presented in Appendix A. While, the explicit expression of the mass matrix ($\boldsymbol{M}$) and force vector ($\boldsymbol{F}_m$) can be found in the Ref. [10].

3.7. Multi-patch technique

In this section, the multi-patch technique and the utilization of bending strip are explained through illustrative diagram. The bending strip technique was proposed by Kiendl et al. [38], in which a strip

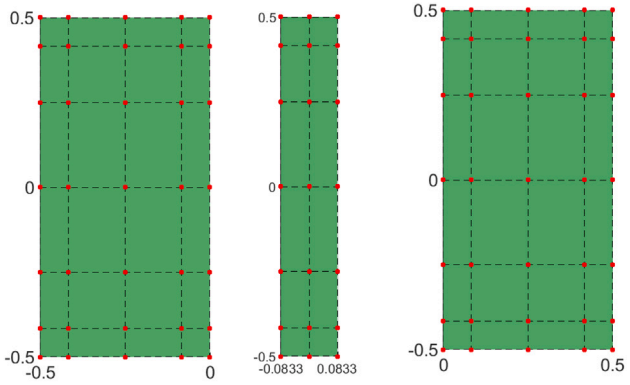

(a) First Patch. **(b)** Bending strip. **(c)** Second Patch.

Fig. 3. Schematic diagram of two patches and bending strip.

of fictitious material with zero mass is placed at the intersection of the patches. Further, it is assumed that the bending strip will only contribute in the direction transverse to bending strip through artificial bending stiffness. This artificial bending stiffness is formed using the penalty technique and then summed with system stiffness matrix. The expression of the penalty stiffness matrix due to bending strip is given as

$$K_{bs}^{\gamma} = \int_{\Omega_{bs}} \left(\boldsymbol{B}_{bs}^{\gamma T} \boldsymbol{D}_{bs}^{\gamma} \boldsymbol{B}_{bs}^{\gamma} \right) d\Omega_{bs}$$

The expression of $\boldsymbol{D}_{bs}^{\gamma}$ depends upon the direction perpendicular to interface (in parametric space). In present study, the expressions of $\boldsymbol{B}_{bs}^{\gamma}$ and $\boldsymbol{D}_{bs}^{\gamma}$ used are given as

$$\begin{Bmatrix} -\frac{\partial^2 w}{\partial \xi^2} \\ -\frac{\partial^2 w}{\partial \eta^2} \\ -2\frac{\partial^2 w}{\partial \xi \partial \eta} \end{Bmatrix} = \sum_{I=1}^{(p+1)(q+1)} \begin{Bmatrix} -\frac{\partial^2 R_I}{\partial \xi^2} \\ -\frac{\partial^2 R_I}{\partial \eta^2} \\ -2\frac{\partial^2 R_I}{\partial \xi \partial \eta} \end{Bmatrix} w_I = \sum_{I=1}^{(p+1)(q+1)} \boldsymbol{B}_{bsI}^{\gamma} \boldsymbol{q}_I = \boldsymbol{B}_{bs}^{\gamma} \boldsymbol{q} \tag{26}$$

$$\boldsymbol{D}_{bs}^{\gamma} = E_2 \times 10^4 \begin{bmatrix} 1 & 0 & 0 \\ 0 & 0 & 0 \\ 0 & 0 & 0 \end{bmatrix}$$

In Fig. 3, the two patches and the bending strip are shown. Further, these patches and the bending strip are combined and presented in Fig. 4. The self explanatory diagrams shown in Figs. 3 and 4 provide exclusive idea of implementing multi-patch technique for the isogeometric approach.

4. Results and discussions

In this section, we will assess the accuracy and efficacy of the proposed IGA model for static and dynamic analysis of multilayered composite plate under hygrothermal environment. In the present investigation, two different types of nonpolynomial shear deformation theories are considered, i.e., inverse hyperbolic shear deformation theory (IHSDT) [21] and inverse hyperbolic tangent shear deformation theory (IHTSDT) [53]. The present theories are selected based on their analytical performance shown in their respective references. Thus, to accomplish this, a MATLAB program is developed to validate the present isogeometric formulation and to carried out further numerical studies. In all upcoming examples, all the solutions (converged) are obtained by considering cubic order NURBS element ($p = 3$) with 12×12 element mesh.

4.1. Material properties

To perform the numerical investigations, various set of material properties given in Tables 1 to 3 are considered. It has been assumed that the thickness and the material properties for all the layers are the same unless stated otherwise.

4.2. Boundary conditions

As present isogeometric formulation is confined to displacement approach; So, only kinematic constraints i.e., $(u_0, v_0, w_0, \theta_x, \theta_y)$ are need to be satisfied for boundary conditions. The different types of boundary conditions, most commonly occurring in practice are considered for numerical investigation of multilayered composite plate and the same are elucidated below.

- Simply supported boundary condition
  1. For cross-ply
     SSSS1: $v_0 = w_0 = \theta_y = 0$ at $x = 0, a$ and $u_0 = w_0 = \theta_x = 0$ at $y = 0, b$
  2. For angle-ply
     SSSS2 : $u_0 = w_0 = \theta_y = 0$ at $x = 0, a$ and $v_0 = w_0 = \theta_x = 0$ at $y = 0, b$
- Clamped boundary condition
  CCCC : $u_0 = v_0 = w_0 = \frac{\partial w_0}{\partial x} = \frac{\partial w_0}{\partial y} = \theta_x = \theta_y = 0$ at $x = 0, a$ and $y = 0, b$
  For restraining the normal slope condition, zero deflection value, i.e., $w_0 = 0$ has been imposed at both control point and control point adjacent to clamped boundary [10].

4.3. Static analysis under hygrothermal environment

This subsection belongs to the description and discussion of various numerically solved examples for establishing the accuracy, efficiency, and applicability of the proposed isogeometric NPSDT model for bending analysis of laminated composite plate under thermal and moisture loads. For comparison purpose, Navier type analytical solutions have also been obtained for IHTSDT and IHSDT by following the procedure given in Appendix B. In addition, 3D elasticity solutions have also been obtained for cross-ply laminated plates by procedure given in [65]. Moreover, for the evaluation of stress-resultants, a continuous least square projection (CL2P) procedure, as described in Ref. [10,66], is utilized.

4.3.1. Bending analysis of cross-ply laminated plates under linear sinusoidal thermal load

In order to validate the present NURBS-based isogeometric formulation for thermo-mechanical bending analysis, an orthotropic plate (0°), a two-layered (0°/90°) and a three-layered (0°/90°/0°) laminated square plates are considered for the investigation. The considered square plates are subjected to sinusoidally distributed transverse mechanical load, $P = P_w \sin\left(\frac{x\pi}{a}\right) \sin\left(\frac{y\pi}{b}\right)$ and thermal load, $\Delta T(x, y, z) = \frac{z}{h} T_1 \sin\left(\frac{\pi x}{a}\right) \sin\left(\frac{\pi y}{b}\right)$ under simply supported ($SSSS1$) boundary condition. The plate is constituted of orthotropic layers having material properties MM1 [57] (in Table 1), where $E_2 = 1$.

The non-dimensional central deflection [21] used in this problem for comparison is defined as

$$\bar{w} = w \left(\left(\frac{P_w a^4}{h^3 \lambda} \right) + \left(\frac{\alpha_{xx} T_1 a^2}{10h} \right) \right)^{-1}$$

where, $\lambda = \left(\frac{\pi^4}{12}\right) \left(4G_{12} + \frac{(E_1 + (1+\nu_{12})E_2)}{1-\nu_{12}\nu_{21}}\right)$.

The non-dimensional central deflection, $\bar{w}$ for various side-to-thickness ratios are obtained using present IGA-IHSDT and IGA-IHTSDT models, and a comparison of present results with the

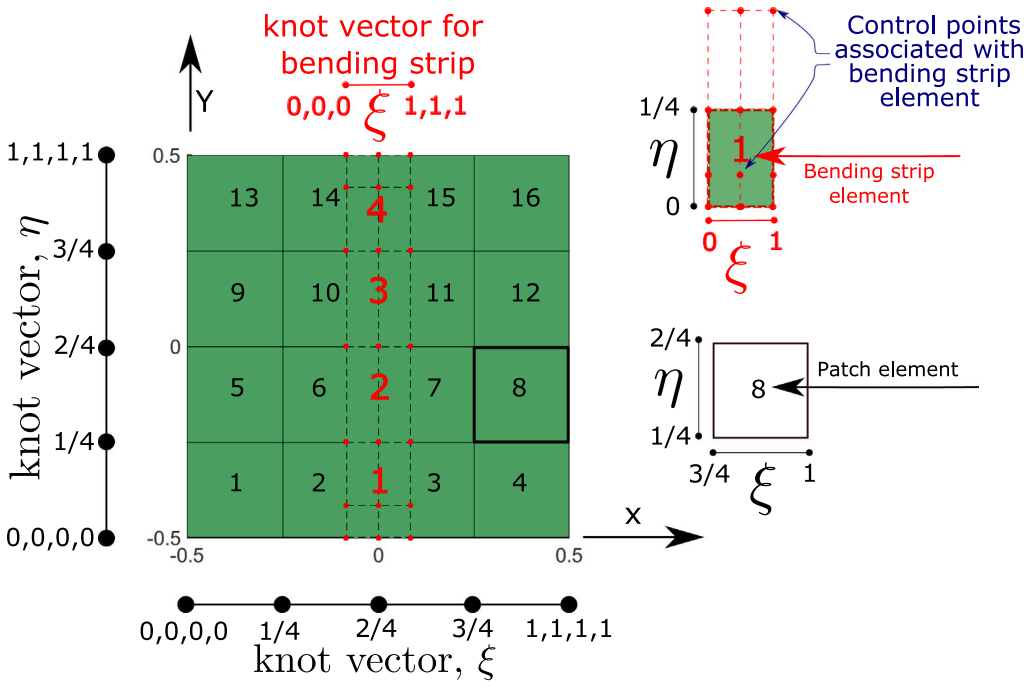

Fig. 4. Schematic diagram of combined patches with bending strip.

Table 1
Material properties used for the analysis of laminated/sandwich composite plate in hygrothermal environment.

Material	Units	E_1	E_2	G_{12}	G_{13}	G_{23}	ν_{12}	ρ	α_1	α_2
	SI	GPa	GPa	GPa	GPa	GPa	–	kg/m^3	1/K	1/K
	FPS	psi	psi	psi	psi	psi	–	lbfs^2/in^4	1/K	1/K
MM1[54,57]	–	$25E_2$	E_2	$0.5E_2$	$0.5E_2$	$0.2E_2$	0.25	–	10^{-6}	$3\alpha_1$
MM2[a][18]	–	–	–	–	G_{12}	$0.5G_{12}$	0.3	–	–	–
MM3[58] Facesheet	SI	200	8	5	5	2.2	0.25	–	-2×10^{-6}	50×10^{-6}
Core		1	1	3.7	0.8	0.8	0.35	–	30×10^{-6}	30×10^{-6}
MM4[59]	SI	$40E_2$	10^{-3}	$0.6E_2$	$0.6E_2$	$0.5E_2$	0.25	1	–	11.4×10^{-6}
MM5[60]	SI	132	10.3	6.5	6.5	3.91	0.3	1570	1.2×10^{-6}	2.4×10^{-6}
MM6[b][26,61]	SI	–	–	–	G_{12}	$0.4E_2$	0.25	1600	–	–
MM7 [62]	SI	$40E_2$	6.895	$0.6E_2$	$0.6E_2$	$0.5E_2$	0.25	3.27	1.14×10^{-6}	11.4×10^{-6}
MM8[62,63]	SI	181	10.3	7.17	7.17	6.21	0.28	1389.23	0.02×10^{-6}	22.5×10^{-6}
MM9[62,64]	FPS	$40E_2$	10^6	$0.6E_2$	$0.6E_2$	$0.5E_2$	0.25	0.00012	1.14×10^{-6}	11.4×10^{-6}

[a]The material properties E_1, E_2 and G_{12} at the elevated temperatures/moisture concentration, shown in Table 2 [18].
[b]The material properties E_1, E_2 and G_{12} at the elevated temperatures/moisture concentration, shown in Table 3 [26,61].

Table 2
Elastic moduli of graphite-epoxy lamina at different temperatures and moisture concentrations with $\alpha_1 = -0.3\times10^{-6}$/K, $\alpha_2 = 28.1\times10^{-6}$/K; $\beta_1 = 0$, $\beta_2 = 0.44$.

(GPa) [a]	Temperature, T (K)					Moisture concentration, C (%)					
	325	350	375	400	425	0.25	0.5	0.75	1.00	1.25	1.50
E_1 130	130	130	130	130	130	130	130	130	130	130	130
E_2 9.5	8.5	8.0	7.5	7.0	6.75	9.25	9.0	8.75	8.5	8.5	8.5
G_{12} 6.0	6.0	5.5	5.0	4.75	4.5	6.0	6.0	6.0	6.0	6.0	6.0

[a]At reference temperature ($T = 300$ K) and moisture concentration ($C = 0$ %).

closed-form solutions [21,57] is shown in Table 4. It is observed from the Table 4 that the present results using IGA-NPSDT model are in close agreement with their respective closed-form solution. The reason for this exemplary performance of IGA-NPSDT can be attributed to the high inter-element continuity of NURBS which simultaneously lead to computational efficient approach in terms of overall solution time [10]. Further, due to the presence of an extensional-bending coupling, the anti-symmetric cross-ply (0°/90°) plate develops prominent thermal moment (M_{yy}) unlike symmetric cross-ply (0° and 0°/90°/0°) plates, and leads to more central-deflection as evident from Table 4. Moreover, in this problem, the thermal coefficients have not been employed through coordinate transformation, i.e., $\alpha_{xx} = \alpha_1$ and $\alpha_{yy} = \alpha_2$ is employed. Further, this problem has been considered under both thermal and mechanical loads with $P_w = 100$ to imitate the practical aspects of loading.

The same example is considered with varying aspect ratio, a/b for a three-layered symmetric cross-ply laminated plate (0°/90°/0°) and the non-dimensional central deflection is evaluated (see Table 5) again under pure thermal load. In this case also, the thermal coefficients have not been undergone the coordinate transformation. It is observed from Table 5 that the present IGA-NPSDT results are in close agreement with the respective closed-form solutions [21]. It is to be emphasized here that the increase in the aspect ratio (a/b), decreases the non-dimensional deflection under the thermal load. This is because the increase in the length of plate decreases the effect of end moments at the center and hence less deflection is observed. Further, the non-dimensional central deflection is obtained for the transformed thermal coefficients and the solutions are shown in Table 6. In Table 6, the solutions have also been obtained for various theories and 3D-Elasticity method to compare the solution with the results presented in Table 5 and to assess the effect of transformation of thermal coefficient. After observing both the Tables 5 and 6, it is evident that the consideration

Table 3
Elastic moduli of carbon-epoxy lamina at different temperatures and moisture concentrations with $\alpha_1 = -0.3 \times 10^{-6}$/K, $\alpha_2 = 28.1 \times 10^{-6}$/K; $\beta_1 = 0$, $\beta_2 = 0.44$.

(GPa)	[a]	Temperature, T (K)					Moisture concentration, C (%)					
		325	350	375	400	425	0.25	0.5	0.75	1.00	1.25	1.50
E_1	172.5	172.5	172.5	172.5	172.5	172.5	172.5	172.5	172.5	172.5	172.5	172.5
E_2	6.9	6.17	5.81	5.45	5.08	4.90	6.72	6.54	6.36	6.17	6.17	6.17
G_{12}	3.45	3.45	3.16	2.88	2.73	2.59	3.45	3.45	3.45	3.45	3.45	3.45

[a]At reference temperature ($T = 300$ K) and moisture concentration ($C = 0$ %).

Table 4
Effect of span-to-thickness ratio and lamination scheme on non-dimensional central deflection of simply supported ($SSSS1$) square laminated plate under sinusoidally distributed transverse load with thermal load, $\Delta T(x, y, z) = \frac{z}{h} T_1 sin\left(\frac{\pi x}{a}\right) sin\left(\frac{\pi y}{b}\right)$, where $T_1 = 100$, $P_w = 100$.

Layer	Source/Method	a/h							
		5	6.25	10	12.5	20	25	50	100
(0°)	CFS-FSDT [57]	2.8332	2.1868	1.4671	1.2973	1.1150	1.0683	1.0105	0.9962
	CFS-IHTSDT	2.7927	2.1696	1.4644	1.2962	1.1113	1.0682	1.0105	0.9960
	IGA-IHTSDT	2.7927	2.1696	1.4644	1.2962	1.1113	1.0682	1.0105	0.9960
	3D-Elasticity	2.7632	2.1526	1.4590	1.2930	1.1102	1.0675	1.0104	0.9960
	CFS-IHSDT [21]	2.7102	2.1244	1.4502	1.2877	1.1082	1.0663	1.0101	0.9959
	IGA-IHSDT	2.7103	2.1245	1.4503	1.2877	1.1083	1.0663	1.0101	0.9959
(0°/90°)	CFS-FSDT [57]	4.0415	3.4666	2.8438	2.7001	2.5443	2.5083	2.4597	2.4454
	3D-Elasticity	3.9345	3.4033	2.8214	2.6861	2.5391	2.5051	2.4598	2.4484
	CFS-IHTSDT	3.8317	3.3372	2.7953	2.6694	2.5326	2.5009	2.4587	2.4482
	IGA-IHTSDT	3.8317	3.3371	2.7953	2.6694	2.5325	2.5009	2.4587	2.4481
	CFS-IHSDT [21]	3.6797	3.2433	2.7602	2.6471	2.5240	2.4955	2.4574	2.4478
	IGA-IHSDT	3.6797	3.2433	2.7602	2.6471	2.5240	2.4955	2.4574	2.4478
(0°/90°/0°)	CFS-FSDT [57]	3.0377	2.9983	1.5384	1.3451	1.1321	1.0811	1.0138	0.9973
	CFS-IHTSDT	3.3133	2.5470	1.6376	1.4118	1.1587	1.0989	1.0183	0.9980
	IGA-IHTSDT	3.3133	2.5470	1.6376	1.4118	1.1587	1.0989	1.0183	0.9980
	CFS-IHSDT [21]	3.4075	2.6317	1.6845	1.4443	1.1726	1.1080	1.0206	0.9966
	IGA-IHSDT	3.4075	2.6317	1.6845	1.4444	1.1426	1.1080	1.0207	0.9986
	3D-Elasticity	3.5058	2.7137	1.7308	1.4771	1.1869	1.1174	1.0231	0.99921

Note: 3D-Elasticity solutions are obtained using procedure given in [65].

of transformation for the thermal coefficients makes a lot of difference in the solution. Therefore, it is essential to make the choice of transformation by considering these aspects of structural design.

4.3.2. Bending analysis of cross-ply laminated plate under linear sinusoidal thermal load for different boundary conditions

Following the previous example, it is important to check the applicability of present model for different boundary conditions other than simply supported one. For this example, material MM1 [54] (given in Table 1) has been considered for the analysis and the following non-dimensional deflection has been used

$$\bar{w} = w(a/2, b/2)\frac{10}{\alpha_1 T_1 b^2}$$

The non-dimensional central deflections of the cross-ply laminated plate have been evaluated for sinusoidally distributed temperature field, $\Delta T(x, y, z) = zT_1 sin\left(\frac{\pi x}{a}\right) sin\left(\frac{\pi y}{b}\right)$ under various boundary conditions and side-to-thickness ratios, (b/h). Lets say ABCDX represents boundary condition, then A at $y = 0$, B at $x = a$, C at $y = b$, and D at $x = 0$ are to be considered while 'X' represents the type of simply supported boundary condition. The obtained results are tabulated in Table 7. For moderately thick plates, the deflection solution predicted for all the mentioned lamination schemes by the IGA-IHSDT and IGA-IHTSDT are in well agreement with available closed-form solutions [54] for various boundary conditions. Further, the accuracy of IHTSDT model is found to almost same as that of TSDT. Also, it can be observed from the results that the deflection in clamped boundary condition is less than the boundary condition having free or simply supported edges. This is because, clamped boundary condition prevents the effect of end thermal moment unlike free boundary condition, which allows the plate to take the end thermal moment.

4.3.3. Bending analysis of anti-symmetric cross-ply laminated plate with temperature and moisture dependent material properties

Till now, for all the problems investigated above, hygrothermal dependent material properties have not been considered. Thus, in this example, the bending characteristics of thin anti-symmetric cross-ply square laminated plate having temperature and moisture dependent material properties subjected to uniform change in temperature, $\Delta T = T - 300 = constant$ and moisture concentration, $\Delta C = C = constant$ is investigated. Each layer of the plate is made of material MM2 [18] (given in Table 1) with side-to-thickness ratio, $a/h = 100$ and $a = b = 0.1$ m. In Table 8, the abbreviations IMP and DMP refer to the hygrothermal independent and dependent material properties, respectively.

For cross-ply laminated plate with $SSSS1$ boundary condition at elevated temperature, $T = 400$ K, the present IGA-NPSDT results are verified with available results [18,44] and new results are also evaluated at various elevated temperatures (see Table 8). Transverse deflections are calculated at points, A(0.5a, 0.5b), B(0.625a, 0.5b), C(0.75a, 0.5b), D(0.875a, 0.5b) and maximum deflection point (0.848a, 0.5b), where a and b are side-lengths as shown in Fig. 2. In this case, no difference in the results of CLPT and NPSDT is observed due to consideration of thin plate, $a/h = 100$. However, a significant difference is observed between results of DMP and IMP, which emphasized the importance of dependent material properties for stress analysis. Moreover, it is observed that due to anti-symmetric $(0^0/90^0/0^0/90^0)$ lamination scheme, the plate deflects in such a way that the central deflection comes out to be zero.

Further, the variation of moments resultants, M_{xx} and M_{yy} for a clamped boundary condition ($CCCC$), at different elevated temperatures, T (K) and moisture concentrations, C (%) are also obtained and shown in Tables 9 and 10, respectively. The obtained isogeometric solutions for moment resultants have been compared with available results and are in good agreement with the same. A monotonically increasing pattern of M_{xx} and M_{yy} are observed with increase in elevated

Table 5
Effect of aspect ratio, a/b and span-to-thickness ratio, a/h on normalized central deflection, $\bar{w} = \left(10w_0h\right)/\left(\alpha_1 T_1 a^2\right)$ of simply supported (SSSS1) square $(0°/90°/0°)$ laminated plate under sinusoidal thermal load, $\Delta T = \left(zT_1/h\right) sin\left(\frac{\pi x}{a}\right) sin\left(\frac{\pi y}{b}\right)$, where $T_1 = 100$, $P_w = 0$ without transformed thermal coefficients.

a/h	Source/Method	$a/b = 1/3$	$a/b = 1/2$	$a/b = 1$	$a/b = 1.5$	$a/b = 2$
5	CFS-FSDT [57]	1.0998	1.1535	1.2224	1.0157	0.7355
	CFS-IHTSDT	1.1073	1.1689	1.2452	1.0169	0.7237
	IGA-IHTSDT	1.1073	1.1689	1.2451	1.0169	0.7237
	CFS-IHSDT [21]	1.1097	1.1740	1.2517	1.0516	0.7187
	IGA-IHSDT	1.1097	1.1740	1.2517	1.0157	0.7187
	3D-Elasticity	1.0676	1.1367	1.2256	0.9908	0.6948
10	CFS-FSDT [57]	1.0701	1.0959	1.1365	0.9973	0.7508
	CFS-IHTSDT	1.0724	1.1008	1.1463	0.9997	0.7455
	IGA-IHTSDT	1.0724	1.1008	1.1463	0.9997	0.7455
	CFS-IHSDT [21]	1.0733	1.1029	1.1507	1.0005	0.7432
	IGA-IHSDT	1.0734	1.1030	1.1507	1.0006	0.7432
	3D-Elasticity	1.0642	1.0953	1.1467	0.9953	0.7362
20	CFS-FSDT [57]	1.0619	1.0795	1.0158	0.9883	0.7601
	CFS-IHTSDT	1.0625	1.0808	1.1087	0.9892	0.7583
	IGA-IHTSDT	1.0625	1.0808	1.1087	0.9892	0.7583
	CFS-IHSDT [21]	1.0628	1.0814	1.1101	0.9896	0.7574
	IGA-IHSDT	1.0628	1.0814	1.1101	0.9896	0.7575
	3D-Elasticity	1.0606	1.0797	1.1094	0.9885	0.7554
50	CFS-FSDT [57]	1.0596	1.0748	1.0963	0.9851	0.7638
	CFS-IHTSDT	1.0597	1.0750	1.0967	0.9853	0.7634
	IGA-IHTSDT	1.0597	1.0750	1.0967	0.9853	0.7634
	CFS-IHSDT [21]	1.0597	1.0750	1.0970	0.9853	0.7632
	IGA-IHSDT	1.0598	1.0751	1.0970	0.9854	0.7633
	3D-Elasticity	1.0594	1.0748	1.0969	0.9852	0.7629
100	CFS-FSDT [57]	1.0593	1.0741	1.0949	0.9847	0.7643
	CFS-IHTSDT	1.0593	1.0741	1.0950	0.9847	0.7642
	IGA-IHTSDT	1.0593	1.0741	1.0950	0.9847	0.7642
	CFS-IHSDT [21]	1.0593	1.0741	1.0950	0.9847	0.7642
	IGA-IHSDT	1.0593	1.0742	1.0950	0.9747	0.7642
	3D-Elasticity	1.0592	1.0741	1.0950	0.9847	0.7641

Note : 3D-Elasticity solutions are obtained using procedure given in [65].

temperature and moisture concentration as also observed in Ref. [18]. Particularly, in this problem, no difference is observed between FSDT and NPSDT results due to consideration of thin plate, $a/h = 100$.

4.3.4. Bending analysis of square sandwich plate under linear sinusoidal thermal load

To show the applicability of present IGA-NPSDT model for sandwich plate, in this example, a three layered $(0°/Core/0°)$ square plate is taken for the analysis [58] which is subjected to thermal load of temperature gradient, $\Delta T(x, y, z) = (z/h) T_1 sin\left(\frac{\pi x}{a}\right) sin\left(\frac{\pi y}{b}\right)$. The facesheets (i.e., layers 1 and 3) and core material (layer 2) are made up of material MM3 [58] as listed in Table 1.

A parametric study for side-to-thickness ratio has been done for simply supported ($SSSS1$) boundary condition taking core thickness (h_c) to be $0.6h$, $0.8h$ or $0.9h$, where h is the plate thickness. A variation of side-to-thickness ratios, a/h ranging from $a/h = 4$ to $a/h = 100$ have been considered, and non-dimensionalized central deflection subjected to thermal load using present IGA-IHSDT and IGA-IHTSDT models are evaluated and tabulated in Table 11. The non-dimensionalized deflections are calculated as $\bar{w} = w(a/2,\ b/2)/(\alpha_0 T_1 h)$, where $\alpha_0 = 10^{-6}$/K and $T_1 = 1$ K. The deflections obtained using present IGA-NPSDT results are found to be close to the available Pagano solution [68] and hence, present IGA-NPSDT model is also capable of predicting the thermoelastic behavior of sandwich plate accurately in the region of 2D plate model. Also, it may be observed that significant difference is found between the 3D elasticity solution and present IGA-NPSDT results for thick sandwich plates. The reason for this difference can be attributed to the contribution of thickness stretching in thick sandwich plate.

4.3.5. Combine effect of temperature and moisture concentration on bending of laminated plate

In all the previous examples, the thermal and moisture loads are applied separately only on cross-ply laminated plates. However, in this problem the combined effect of temperature and moisture on the bending response is assessed on angle-ply laminated plates. To employ this, the temperature and moisture variations have been considered as $\Delta T = T_0 + zT_1/h + f(z)T_2/h$ and $\Delta C = C_0 + zC_1/h + f(z)C_2/h$, respectively. The laminated plate with side-to-thickness ratio, $a/h = 5$ is made of materials as follows: $E_0 = 1$ GPa, $E_1 = 15E_0$, $E_2 = E_3 = 6E_0$, $G_{12} = G_{13} = 3E_0$, $G_{23} = 1.5E_0$, $\nu_{12} = \nu_{13} = \nu_{23} = 0.3$, $\alpha_0 = 10^{-6}$/K, $\alpha_1 = 7\alpha_0$, $\alpha_2 = \alpha_3 = 23\alpha_0$, $\beta_0 = 1\,(wt.\%\ H_2O)^{-1}$, $\beta_1 = 0$, $\beta_2 = \beta_3 = 0.6\beta_0$ [74]. The obtained non-dimensionalized central deflection ($\bar{w} = w/\alpha_0 T_1 h$) for the four-layered angle-ply laminated clamped (CCCC) plate is shown in Table 12. It can be observed that present IGA-NPSDT results are found to be in accordance with available HPT and SPT results [74]. However, little discrepancies in the results are observed. The reason for this discrepancy can be attributed to the different shear deformation theory used in the analysis.

4.4. Dynamic analysis under hygrothermal environment

In this subsection, the dynamic analysis of an initially stressed composite plate has been carried out using the proposed IGA-NPSDT model. The stress stiffening effect generated due to initial hygrothermal load has been incorporated through both von Kármán and Green–Lagrange strain relationships. Also, a comparison is made between both the nonlinearity to have a clear understanding of the same on multilayered composite plate. In the first half, free vibration analysis, and in the second part, forced vibration analysis has been conducted, followed by validation. The forced vibration includes transient damped and steady-state harmonic solution. The fast Fourier transform analysis has also been carried out to provide a holistic analysis in frequency domain. Here, the transient response of plates is obtained by using constant average acceleration Newmark's time integration method [10].

Table 6
Effect of aspect ratio, a/b and span-to-thickness ratio, a/h on normalized central deflection, $\bar{w} = (10w_0h)/(\alpha_1 T_1 a^2)$ of simply supported (SSSS1) square $(0°/90°/0°)$ laminated plate under sinusoidal thermal load, $\Delta T = (zT_1/h)\sin\left(\frac{\pi x}{a}\right)\sin\left(\frac{\pi y}{b}\right)$, where $T_1 = 100$, $P_w = 0$ with transformed thermal coefficients.

a/h	Source/Method	$a/b = 1/3$	$a/b = 1/2$	$a/b = 1$	$a/b = 1.5$	$a/b = 2$
5	IGA-FSDT	1.07677	1.10193	1.07630	0.84211	0.58736
	CFS-IHTSDT	1.07970	1.10960	1.08740	0.84240	0.58582
	IGA-IHTSDT	1.07971	1.10964	1.08735	0.84240	0.58582
	CFS-IHSDT	1.07980	1.11160	1.09150	0.84510	0.58955
	IGA-IHSDT	1.07983	1.11161	1.09150	0.84510	0.58955
	3D-Elasticity	1.03470	1.06880	1.05340	0.80740	0.55194
10	IGA-FSDT	1.05938	1.06974	1.04602	0.86426	0.62022
	CFS-IHTSDT	1.06030	1.07220	1.04990	0.86179	0.61413
	IGA-IHTSDT	1.06032	1.07216	1.04986	0.86179	0.61413
	CFS-IHSDT	1.06050	1.07310	1.05160	0.86111	0.61246
	IGA-IHSDT	1.06054	1.07309	1.05158	0.86111	0.61246
	3D-Elasticity	1.05040	1.06380	1.04350	0.85136	0.60214
20	IGA-FSDT	1.05463	1.06059	1.03520	0.87500	0.64031
	CFS-IHTSDT	1.05490	1.06120	1.03630	0.87401	0.63764
	IGA-IHTSDT	1.05488	1.06123	1.03627	0.87401	0.63764
	CFS-IHSDT	1.05490	1.06150	1.03680	0.87360	0.63659
	IGA-IHSDT	1.05495	1.06150	1.03677	0.87360	0.63659
	3D-Elasticity	1.0525	1.05930	1.03490	0.87097	0.63342
50	IGA-FSDT	1.05327	1.05794	1.03183	0.87877	0.64820
	CFS-IHTSDT	1.05330	1.05800	1.03200	0.87859	0.64769
	IGA-IHTSDT	1.05331	1.05804	1.03201	0.878593	0.64769
	CFS-IHSDT	1.05330	1.05810	1.03210	0.87851	0.64747
	IGA-IHSDT	1.05332	1.05809	1.03209	0.87851	0.64748
	3D-Elasticity	1.05290	1.05770	1.03180	0.87808	0.64691
100	IGA-FSDT	1.05307	1.05756	1.03134	0.87935	0.64944
	CFS-IHTSDT	1.0531	1.0576	1.0314	0.8793	0.64931
	IGA-IHTSDT	1.05308	1.05758	1.03138	0.879301	0.64931
	CFS-IHSDT	1.05310	1.0576	1.0314	0.87928	0.64926
	IGA-IHSDT	1.05308	1.05760	1.03140	0.879281	0.64926
	3D-Elasticity	1.05300	1.0575	1.0313	0.87917	0.64911

Note : 3D-Elasticity solutions are obtained using procedure given in [65].

Table 7
Effect of boundary conditions and span-to-thickness ratio on non-dimensional central deflection of cross-ply square laminated plate subjected to thermal load, $\Delta T = zT_1 \sin(\pi x/a)\sin(\pi y/b)$.

Layer	a/h	Source/Method	SSSS1	SCSS1	SCSC1	SFSF1	SSSF1	CCCC
(0°)	5	CFS-FSDT [54]	1.0721	0.7613	0.3913	2.2894	1.5859	–
		CFS-TSDT [54]	1.0711	0.7175	0.3663	2.2812	1.5831	–
		IGA-IHTSDT	1.0711	0.7147	0.3647	2.2895	1.5857	0.3062
		IGA-IHSDT	1.0693	0.6921	0.3516	2.2898	1.5859	0.3009
	10	CFS-FSDT [54]	1.0440	0.5677	0.2912	2.2928	1.5952	–
		CFS-TSDT [54]	1.0439	0.5587	0.2871	2.2854	1.5931	–
		IGA-IHTSDT	1.0439	0.5566	0.2862	2.2928	1.5953	0.2750
		IGA-IHSDT	1.0435	0.5515	0.2838	2.2929	1.5955	0.2735
(0°/90°)	5	CFS-FSDT [54]	1.1504	0.8547	0.6231	1.2784	1.2170	–
		CFS-TSDT [54]	1.1430	0.8190	0.5814	1.2652	1.2068	–
		IGA-IHTSDT	1.1429	0.8171	0.5790	1.2670	1.2077	0.3042
		IGA-IHSDT	1.1395	0.8004	0.5601	1.2615	1.2035	0.2990
	10	CFS-FSDT [54]	1.1504	0.7703	0.5307	1.2736	1.2176	–
		CFS-TSDT [54]	1.1485	0.7586	0.5164	1.2693	1.2145	–
		IGA-IHTSDT	1.1485	0.7574	0.5150	1.2706	1.2152	0.3132
		IGA-IHSDT	1.1476	0.7516	0.5080	1.2691	1.2141	0.3116
(0°/90°/0°)	5	CFS-FSDT [54]	1.0763	0.8155	0.4578	1.6597	1.3698	–
		CFS-TSDT [54]	1.0874	0.8032	0.4556	1.6687	1.3805	–
		IGA-IHTSDT	1.0873	0.8002	0.4533	1.6729	1.3823	0.3150
		IGA-IHSDT	1.0915	0.7893	0.4468	1.6818	1.3891	0.3165
	10	CFS-FSDT [54]	1.0460	0.6037	0.3211	1.6640	1.3737	–
		CFS-TSDT [54]	1.0499	0.6142	0.3275	1.6632	1.3757	–
		IGA-IHTSDT	1.0499	0.6115	0.3259	1.6671	1.3774	0.2839
		IGA-IHSDT	1.0516	0.6163	0.3287	1.6691	1.3794	0.2853

4.4.1. Free vibration analysis of cross-ply laminated plate for different thermal expansion coefficient ratio

In this first example, a four-layered square laminated plate with side-to-thickness ratio, $a/h = 10$, subjected to a uniform temperature change $\Delta T = T_0$ is considered for free vibration analysis. The plate is composed of material MM4 [59] (given in Table 1) with temperature independent material properties. The non-dimensionalized natural frequency, $\bar{\omega} = \omega\left(a^2/h\right)\sqrt{\rho/E_2}$ for simply supported, $SSSS2$ boundary condition is shown in Table 13. From Table 13, one can conclude that non-dimensional frequencies predicted by IGA-IHTSDT are found to be more accurate than IGA-IHSDT which even over predicts the IGA-FSDT solution. Thus, based on the results listed one can conclude that it is necessary to validate the efficiency of NPSDT model for both static and dynamic analysis for accurate modeling. Further, it has been observed that the non-dimensional frequencies changes almost linearly with the change of temperature for all cases, and present results are in good agreement with the available solutions [59]. Furthermore, it can be noticed from the Table 13 that there is not much difference observed in natural frequencies for von Kármán and Green–Lagrange nonlinearity. This is due to the applied temperature in present problem being just 0.3% of the critical buckling temperature of the plate. Moreover, it has been checked in subsequent results that with higher temperature change, a significant difference between these two nonlinearities has been observed, specifically near buckling temperature.

4.4.2. Free vibration analysis of symmetric cross-ply clamped laminated plate under uniform thermal load

The study of first few modes of vibration are enough to assess the properties of any structure, and these modes need to be accurately predicted by present IGA-NPSDT model. To demonstrate this, a clamped rectangular laminated plate with dimensions $600 \times 400 \times 5$ mm^3 and subjected to uniform temperature change, $\Delta T = T_0$ is considered for free vibration analysis. The plate is composed of five layers, $(0°/90°/0°/90°/0°)$ with material properties MM5 [60] (listed in Table 1). The variation of natural frequencies (in Hz) with respect to change in temperature is shown in Table 14. The von Kármán nonlinearity is employed to obtain present IGA-FSDT and IGA-IHTSDT solutions. The obtained solutions are found to be in good agreement with the available solution [60].

Further, multi-patch technique plays a pivotal role in isogeometric analysis as complete geometry of any practical structure cannot be easily achieved by single patch geometry. Therefore, the solutions have been obtained by considering the multi-patch with/without bending strip. The effect of single and multi-patch with/without bending strip is shown in Table 14. The solution also includes the actual FSDT and the FSDT derived from HSDT by using $f(z) = z$. It is observed that the solution obtained from FSDT, which is derived from $f(z) = z$, is erroneous for multi-patch geometry without bending strip. Whereas, the actual FSDT solution for single patch, and multi-patch with/without bending strip gives a correct solution. Further, the solution obtained from IGA-FSDT (FSDT derived by putting $f(z) = z$) for single or multi-patch with bending strip also gives correct solution as marked by ^{b} in Table 14. Further, in case of IGA-IHSDT model, when multi-patch without bending strip is used, erroneous result is observed. Whereas, IGA-IHSDT for single and multi-patch model with bending strip gives an accurate result as marked by ^{d} in Table 14. Hence, it is quite evident that the bending strip is essential to get the accurate solution for HSDT due to the requirement of C^1 continuity. However, the actual FSDT is immune to the bending strip due to the requirement of C^0 continuity which is naturally satisfied by only multi-patches (without bending strip). Moreover, bending strip can still be applied with actual FSDT as it will not alter the solution.

Further, the effect of multi-patch technique with/without bending strip is presented by mode shapes as shown in Fig. 5. It is observed from Fig. 5a that multi-patch without bending strip creates a sharp kink in the central plate. Whereas, multi-patch with bending strip and the single-patch creates a smooth mode shape profile as shown in Fig. 5b.

Table 8
Deflection (in mm) of simply supported anti-symmetric $(0°/90°/0°/90°)$ square laminated plate at elevated temperature, T with $a = b = 0.1$ m, $a/h = 100$.

T (K)	Material	Source/ Model	A $\left(0.5a, \frac{b}{2}\right)$	B $\left(0.625a, \frac{b}{2}\right)$	C $\left(0.75a, \frac{b}{2}\right)$	D $\left(0.875a, \frac{b}{2}\right)$	Max. $\left(0.848a, \frac{b}{2}\right)$
325	IMP	IGA-IHTSDT	0	0.00270	0.00845	0.010733	0.01098
		IGA-IHSDT	0	0.00270	0.00846	0.010747	0.01099
		CFS-CLPT*	0	0.00270	0.00846	0.010729	0.01097
	DMP	IGA-IHTSDT	0	0.00247	0.00774	0.00982	0.01005
		IGA-IHSDT	0	0.00247	0.00775	0.00982	0.01006
		CFS-CLPT*	0	0.00247	0.00775	0.00982	0.01005
350	IMP	IGA-IHTSDT	0	0.00539	0.01691	0.02147	0.02197
		IGA-IHSDT	0	0.00539	0.01692	0.02149	0.02199
		CFS-CLPT*	0	0.00540	0.01693	0.02145	0.02194
	DMP	IGA-IHTSDT	0	0.00473	0.01480	0.01875	0.01920
		IGA-IHSDT	0	0.00473	0.01481	0.01876	0.01922
		CFS-CLPT*	0	0.00474	0.01482	0.01876	0.01919
375	IMP	IGA-IHTSDT	0	0.00809	0.02536	0.03220	0.03296
		IGA-IHSDT	0	0.00809	0.02538	0.03224	0.03299
		CFS-CLPT*	0	0.00810	0.02539	0.03218	0.03218
	DMP	IGA-IHTSDT	0	0.00676	0.02114	0.02675	0.02740
		IGA-IHSDT	0	0.00677	0.02116	0.02677	0.02743
		CFS-CLPT*	0	0.00677	0.02117	0.02676	0.02738
400	IMP	IGA-IHTSDT	0	0.01078	0.03382	0.04294	0.04394
		IGA-IHSDT	0	0.01079	0.03384	0.04298	0.04399
		CFS-CLPT*	0	0.01080	0.03386	0.04292	0.04388
	DMP	IGA-IHTSDT	0	0.00854	0.02668	0.03373	0.03456
		IGA-IHSDT	0	0.00854	0.02671	0.03375	0.03460
		CFS-CLPT [67]	–	0.00850	0.02670	0.03370	–
		CFS-CLPT*	0	0.00855	0.02672	0.03374	0.03453
425	IMP	IGA-IHTSDT	0	0.01347	0.04227	0.05367	0.05493
		IGA-IHSDT	0	0.01349	0.04230	0.05373	0.05499
		CFS-CLPT*	0	0.01351	0.04232	0.05365	0.05485
	DMP	IGA-IHTSDT	0	0.01038	0.03242	0.04095	0.04197
		IGA-IHSDT	0	0.01039	0.03245	0.04099	0.04201
		CFS-CLPT*	0	0.01039	0.03246	0.04097	0.04194

Note : For IMP, material properties correspond to $T = 300$ K.
*Present closed-form results are obtained using procedure given in Ref. [67].

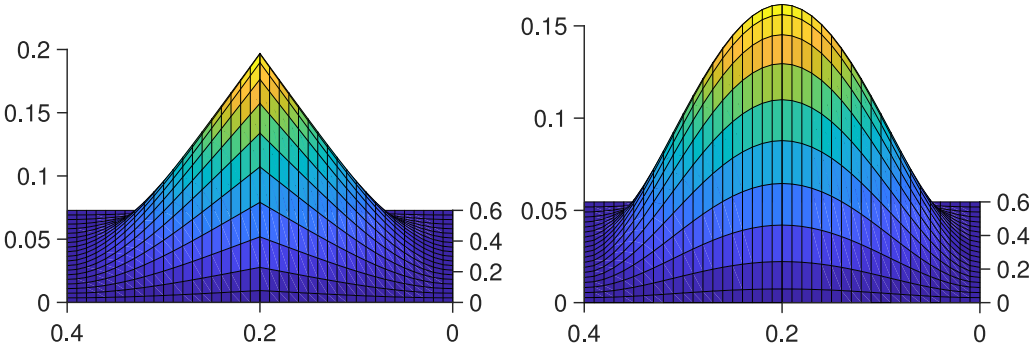

(a) Without bending strip. **(b)** With bending strip.

Fig. 5. First mode shape with and without bending strip using HSDT.

Table 9
Moment resultant variation of clamped $(CCCC)$ anti-symmetric $(0°/90°/0°/90°)$ square laminated plate at elevated temperature, T (K) $a = b = 0.1$ m, $a/h = 100$.

Moment (N mm)	Source/Method	Temperature (K) 325	350	375	400	425
M_{xx}	FEM_FSDT [18]	−0.3230	−0.6150	−0.8760	−1.1060	−1.3440
	IGA-FSDT [44]	−0.3229	−0.6146	−0.8757	−1.1057	−1.3435
	IGA-IHTSDT	−0.3229	−0.6148	−0.8757	−1.1057	−1.3435
	IGA-IHSDT	−0.3229	−0.6148	−0.8757	−1.1057	−1.3435
M_{yy}	FEM_FSDT [18]	0.3230	0.6150	0.8760	1.1060	1.3440
	IGA-FSDT [44]	0.3230	0.6150	0.8760	1.1060	1.3440
	IGA-IHTSDT	0.3229	0.6148	0.8757	1.1057	1.3435
	IGA-IHSDT	0.3229	0.6148	0.8757	1.1057	1.3435

Table 10
Moment resultant variation of clamped $(CCCC)$ anti-symmetric $(0°/90°/0°/90°)$ square laminated plate at elevated moisture concentration, C (%) $a = b = 0.1$ m, $a/h = 100$.

Moment (N mm)	Source/Method	Moisture concentration (%) 0.25	0.5	0.75	1.0	1.25	1.5
M_{xx}	FEM_FSDT [18]	−0.448	−0.872	−1.271	−1.646	−2.057	−2.469
	IGA-IHTSDT	−0.448	−0.872	−1.271	−1.646	−2.057	−2.469
	IGA-IHSDT	−0.448	−0.872	−1.271	−1.646	−2.057	−2.469
M_{yy}	FEM-FSDT [18]	0.448	0.872	1.271	1.646	2.057	2.469
	IGA-IHTSDT	0.448	0.872	1.271	1.646	2.057	2.469
	IGA-IHSDT	0.448	0.872	1.271	1.646	2.057	2.469

Table 11
Normalized central deflection, $\bar{w} = w/\left(\alpha_0 T_1 h^2\right)$ of simply supported (SSSS1) square sandwich plate subjected to linear thermal load, $\Delta T = zT_1 sin\left(\frac{\pi x}{a}\right) sin\left(\frac{\pi y}{b}\right)$ corresponding to span-to-thickness ratio, a/h and core-to-thickness ratio, h_c/h.

h_c/h	Source/	a/h							
	Method	4	5	8	10	12	20	50	100
0.6	Cetkovic [69]	12.671	–	21.521	–	28.512	43.278	–	–
	Padhi and Pandit [70]	9.352	–	19.435	–	26.317	41.428	–	–
	Shariyat [71]	9.290	–	19.317	–	26.292	41.398	–	–
	Matsunaga [72]	8.793	–	18.780	–	25.640	40.630	–	–
	Pagano [73]	9.816	–	19.870	–	26.960	42.180	–	–
	3D-Elasticity	9.181	12.484	19.808	23.521	26.963	42.181	152.24	541.77
	IGA-IHSDT	10.159	12.901	19.001	22.237	25.366	40.042	149.80	539.28
	IGA-IHTSDT	9.238	11.606	16.935	19.885	22.830	37.195	146.78	536.24
0.8	3D-Elasticity	7.968	10.384	16.316	20.046	24.035	44.873	208.84	792.82
	IGA-IHSDT	8.960	11.037	16.323	19.826	23.671	44.271	208.11	792.07
	IGA-IHTSDT	9.106	11.301	16.826	20.414	24.314	45.004	208.89	792.86
0.9	3D-Elasticity	5.671	7.627	13.773	18.638	24.340	56.546	317.98	1251.0
	IGA-IHSDT	6.509	8.203	13.906	18.629	24.246	56.315	317.67	1250.7
	IGA-IHTSDT	6.908	8.729	14.647	19.438	25.095	57.229	318.62	1251.7

Note: 3D-Elasticity solutions are obtained using procedure given in [65].

Table 12
Normalized central deflection, $\bar{w} = w/\alpha_0 T_1 h$ of four layered square laminated clamped (CCCC) plate under hygrothermal effect with $a/h = 5$; $\alpha_{xx} = m^2\alpha_1 + n^2\alpha_2$; $\alpha_{yy} = n^2\alpha_1 + m^2\alpha_2$; $\alpha_{xy} = mn\alpha_1 - mn\alpha_2$; $m = cos\left(\theta_k\right)$; $n = sin\left(\theta_k\right)$.

Hygrothermal condition	Laminate	Source/Model				
		IHSDT	IHTSDT	HPT [74]	SPT [74]	HGLM [74]
$T_0 = 100$ K; $T_1 = T_2 = 0$ $C_0 = 0.01\%$; $C_1 = C_2 = 0$	(65°/25°/25°/65°)	0.000	0.000	0.000	0.000	52.703
$T_0 = T_1 = 100$ K; $T_2 = 0$ $C_0 = C_1 = 0.01\%$; $C_2 = 0$	(65°/25°/25°/65°)	22.050	22.055	22.423	22.436	85.013
$T_0 = T_1 = T_2 = 100$ K	(65°/25°/25°/65°)	39.419	39.499	39.559	39.562	109.700
$C_0 = C_1 = C_2 = 0.01\%$	(85°/5°/5°/85°)	37.126	36.982	36.123	36.260	29.966
	(65°/15°/15°/65°)	40.059	40.059	39.275	39.274	33.160
	(45°/25°/25°/45°)	42.259	42.391	41.649	41.649	36.014

HGLM stands for higher-order global–local model; values are extract from the figure shown in [74].
HPT and SPT refer to higher-order and sinusoidal shear deformation theories, respectively.

Table 13
Normalized natural frequency of a simply supported ($SSSS2$) laminated plate $(0°/90°)_s$ subjected to uniform temperature change, $\Delta T = T_0$.

Source/Method		$\alpha_1/\alpha_2 = -0.05$		$\alpha_1/\alpha_2 = 0.1$		$\alpha_1/\alpha_2 = 0.2$		$\alpha_1/\alpha_2 = 0.5$	
	$\Delta T = 0$	$\Delta T = -50$	$\Delta T = 50$	$\Delta T = -50$	$\Delta T = 50$	$\Delta T = -50$	$\Delta T = 50$	$\Delta T = -50$	$\Delta T = 50$
Naidu and Sinha [55]	15.1480	–	–	–	15.0985	–	–	–	–
FEM-FSDT [59]	15.1500	15.1360	15.1640	15.2470	15.0520	15.3200	14.9780	15.3940	14.9020
IGA-FSDT[a]	15.1426	15.1286	15.1567	15.2395	15.0451	15.3131	14.9703	15.5316	14.7434
IGA-FSDT[b]	15.1426	15.1284	15.1567	15.2404	15.0441	15.3146	14.9685	15.5351	14.7395
IGA-IHTSDT[a]	15.1073	15.0932	15.1214	15.2045	15.0096	15.2782	14.9345	15.4972	14.7071
IGA-IHTSDT[b]	15.1073	15.0931	15.1215	15.2054	15.0086	15.2798	14.9329	15.5008	14.7033
IGA-IHSDT[a]	15.1844	15.1704	15.1984	15.2810	15.0871	15.3544	15.0125	15.5723	14.7863
IGA-IHSDT[b]	15.1844	15.1702	15.1985	15.2819	15.0862	15.3560	15.0109	15.5759	14.7825

[a]Present von Kármán solution.
[b]Present Green–Lagrange solution.

4.4.3. Effect of side-to-thickness ratio on free vibration characteristic

In this example, two simply supported square laminated plate subjected to uniform temperature environment is considered for free vibration analysis. The plate having constant thickness ($h = 50.8$ mm) is made of orthotropic material with temperature independent material property MM7 [62] (listed in Table 1). All the four edges of the plate are assumed to be simply supported with no in-plane displacement, i.e., $SSSS2$. In Table 15, the effect of side-to-thickness ratio on the non-dimensional natural frequency at different exposed temperature is tabulated. Based on the results listed in Table 15, one can conclude that IGA-IHTSDT results found to be better than the available solution [62] due to the consideration of pre-buckling stress distribution in present approach in compare to assumed thermal stress resultant in Ref. [62]. Further, it is seen that the degradation in the natural frequency is found to be more in thin plate than thick plate. However, a very small difference is observed between von Kármán and Green–Lagrange results as considered change in temperature (ΔT) is just $\frac{1}{6}$th and $\frac{1}{10}$th of the critical buckling temperature for cross-ply (1232.26 K) and angle-ply (2005.2 K) laminated plates, respectively. Moreover, the natural frequency is also obtained through fast Fourier transform (FFT) approach from time-domain solution (as demonstrated in Section 4.4.6), and the obtained solutions are in well agreement with other approaches.

4.4.4. Free vibration analysis of anti-symmetric angle-ply laminated plate around critical buckling temperature

In this example, an anti-symmetric angle-ply square laminated plate with side-to-thickness ratio, $a/h = 10$ subjected to a uniform thermal environment (ΔT) is considered for free vibration analysis. The plate consists of four layers $(45°/-45°)_2$ having material properties MM8 [62,63] (listed in Table 1) restrained by $SSSS2$ simply supported boundary condition. The constant temperature difference, ΔT varies from 0, $0.25T_*$, $0.5T_*$ and $0.75T_*$, where $T_* = 1656.72/(\alpha_2 \times 10^4)$. The non-dimensional natural frequencies, ω/ω_0 for present IGA-FSDT, IGA-IHSDT and IGA-IHTSDT models using both nonlinearities are shown

Table 14
Effect of temperature on natural frequencies (Hz) of a clamped rectangular laminated $(0°/90°/0°/90°/0°)$ plate under uniform temperature change, $\Delta T = T_0$.

Mode	Source/Model	$\Delta T = T_0$					Mode	$\Delta T = T_0$				
		0	20	40	60	80		0	20	40	60	80
(1,1)	Nastran [60]	200.02	176.91	149.89	116.19	66.10	(2,2)	564.53	535.09	503.80	470.28	433.99
	IGA-FSDT[a]	162.18	118.97	7.02	×	×		565.29	535.86	504.59	447.11	371.69
	IGA-FSDT[b]	200.17	177.05	150.03	116.36	66.39		565.29	535.86	504.59	471.09	434.86
	IGA-IHTSDT[c]	162.17	118.96	6.72	×	×		564.97	535.54	504.25	446.34	370.87
	IGA-IHTSDT[d]	200.19	176.99	149.97	116.28	66.25		564.97	535.54	504.25	470.75	434.49
(2,1)	Nastran [60]	371.52	349.48	325.79	300.03	271.57	(3,1)	664.94	644.20	622.71	600.38	577.11
	IGA-FSDT[a]	353.67	326.44	294.60	254.82	198.36		631.20	576.35	515.33	471.09	434.86
	IGA-FSDT[b]	371.69	349.65	325.95	300.19	271.74		665.19	644.43	622.93	600.59	577.32
	IGA-IHTSDT[c]	353.69	326.46	294.62	254.83	198.32		630.53	575.66	514.61	470.75	434.49
	IGA-IHTSDT[d]	371.69	349.65	325.95	300.19	271.74		665.28	644.53	623.03	600.70	577.43
(1,2)	Nastran [60]	447.63	418.46	386.92	352.35	313.74	(3,2)	808.77	771.35	752.85	723.15	692.09
	IGA-FSDT[a]	448.29	419.13	387.61	353.09	314.55		655.71	633.09	609.10	580.71	514.33
	IGA-FSDT[b]	448.29	419.13	387.61	353.09	314.55		809.62	782.19	753.70	724.02	692.98
	IGA-IHTSDT[c]	447.90	418.73	387.19	352.63	314.05		655.81	633.20	609.22	580.02	513.61
	IGA-IHTSDT[d]	447.90	418.73	387.19	352.63	314.05		809.45	782.03	753.54	723.85	692.81

[a]IGA-FSDT model using $f(z) = z$ and shear correction factor in transverse energy, multi-patch without bending strip.
[b]IGA-FSDT (actual FSDT) model for single patch.
IGA-FSDT (actual FSDT) model for multi patch with or without bending strip.
IGA-FSDT (FSDT derived from HSDT with $f(z) = z$) model for single or multi patch with bending strip.
[c]Multi patch without bending strip.
[d]Single patch or multi path with bending strip.

Table 15
Non-dimensional natural frequency, $\bar{\omega} = \omega\left(a^2/h\right)\sqrt{\rho/E_2}$ of simply supported $(SSSS2)$ laminated square plates subjected to uniform temperature change, ΔT.

ΔT	Source/Method	$(0°/90°/0°)$				$(45°/-45°)_2$			
		$a/h = 5$	$a/h = 10$	$a/h = 20$	$a/h = 50$	$a/h = 5$	$a/h = 10$	$a/h = 20$	$a/h = 50$
0	TSDT[c] [62]	10.263	14.702	17.483	18.689	12.544	18.333	21.812	23.225
	IGA-IHTSDT	10.2632	14.7025	17.4832	18.6408	12.5333	18.3223	21.8064	23.2237
	IGA-IHSDT	10.3698	14.7519	17.4998	18.6438	12.5835	18.3100	21.7957	23.2214
	FFT[d]	10.369	14.736	17.538	18.756	12.582	18.322	21.805	23.23
100	TSDT[c] [62]	10.226	14.597	17.172	16.412	12.513	18.248	21.524	21.477
	IGA-IHTSDT[a]	10.1923	14.501	16.7918	14.1055	12.4744	18.1606	21.2562	19.7697
	IGA-IHTSDT[b]	10.1905	14.4990	16.7894	14.1021	12.4740	18.1596	21.2546	19.7675
	IGA-IHSDT[a]	10.2996	14.5511	16.8092	14.1094	12.5249	18.1483	21.2452	19.7669
	IGA-IHSDT[b]	10.2979	14.5490	16.8067	14.1061	12.5245	18.1473	21.2436	19.7647
	FFT[d]	10.299	14.550	16.877	14.282	12.523	18.150	21.309	19.788
200	TSDT[c] [62]	10.188	14.490	16.856	13.828	12.482	18.163	21.233	19.574
	IGA-IHTSDT[a]	10.1209	14.2967	16.0708	7.1029	12.4151	17.9974	20.6914	15.5673
	IGA-IHTSDT[b]	10.1174	14.2925	16.0657	7.0895	12.4144	17.9955	20.6881	15.5616
	IGA-IHSDT[a]	10.2290	14.3474	16.0889	7.1107	12.4661	17.9851	20.6802	15.5638
	IGA-IHSDT[b]	10.2254	14.3433	16.0838	7.09735	12.4652	17.9830	20.6768	15.5581
	FFT[d]	10.228	14.420	16.271	7.5712	12.465	17.985	20.841	15.486

[a]Present von Kármán solution.
[b]Present Green–Lagrange solution.
[c]Solution using state variable approach.
[d]Fast Fourier transformation of time domain response of IGA-IHSDT (von Kármán).

in Table 16 with $\omega_0 = \left(\left(h^2/a^4\right)\left(E_{22}/\rho\left(1-\nu_{12}\nu_{21}\right)\right)\right)^{1/2}$. It is apparent from the solutions that the present results using NURBS-based IGA model are found to be better than the available TSDT results of Shen et al. [62] and Chandrashekhara [63] as they are over predicting the solution. The reason for better results is due to the consideration of pre-buckling stress distribution in geometric stiffness matrix in present approach while Shen et al. [62] and Chandrashekhara [63] considered the assumed thermal stress resultant in their approach. Particularly, a significant difference is observed between Green–Lagrange and von Kármán nonlinear results with increase in temperature, specifically around critical buckling temperature. This emphasize the use of Green–Lagrange nonlinearity for stress stiffening effect at higher temperature change.

Further, to show the profound difference between Green–Lagrange and von Kármán stress solution, the same example is repeated for thick plate $(a/h = 4)$ and obtained results are tabulated in Table 17. Here the

Table 16
Comparisons of non-dimensional natural frequencies, ω/ω_0 for laminated square plate $(45°/-45°)_2$ under various ΔT.

Source/Method	Temperature ΔT				
	0	$0.25T_*$	$0.5T_*$	$0.75T_*$	$0.9T_*$
Chandrashekhara et al. [63]	14.4382	12.5038	10.2093	7.2191	–
Shen et al. [62]	14.3116	12.3788	10.0819	7.0750	–
IGA-FSDT[a]	14.2883	12.3219	9.9751	6.8683	3.9719
IGA-FSDT[b]	14.2883	12.2914	9.8996	6.7027	3.6166
IGA-IHTSDT[a]	14.2359	12.2612	9.9001	6.7591	3.7801
IGA-IHTSDT[b]	14.2359	12.2302	9.8233	6.5891	3.4010
IGA-IHSDT[a]	14.2327	12.2578	9.8963	6.7541	3.7718
IGA-IHSDT[b]	14.2327	12.2264	9.8183	6.5812	3.3852

[a]Present von Kármán solution.
[b]Present Green–Lagrange solution.

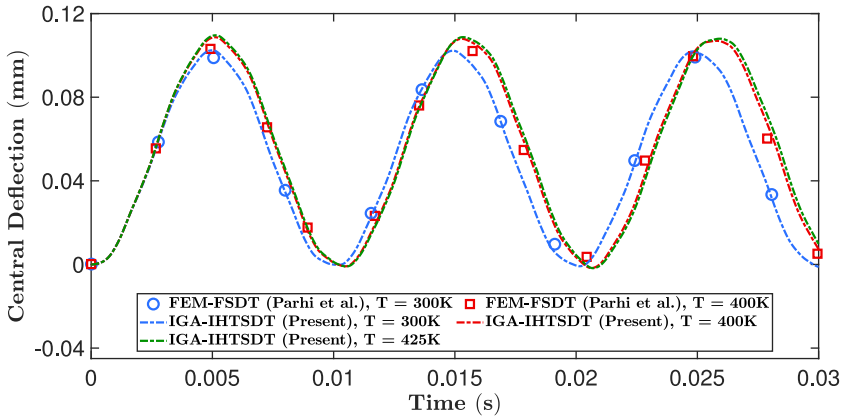

Fig. 6. Central deflection of twenty-layered cross-ply laminate $(0°/90°)_{10}$ plate subjected to uniformly distributed step loading with uniform thermal environment under simply supported ($SSSS1$) boundary condition for temperature, $T = 300$ K, 400 K and 425 K.

Table 17
Comparisons of natural frequencies (in Hz) for thick $(a/h = 4)$ laminated square plate $(45°/-45°)_2$ under various ΔT.

Source/Method	$T_\lambda(K)$	Temperature ΔT				
		0	$0.25T_*$	$0.5T_*$	$0.75T_*$	T_*
IGA-FSDT[a]	22 220	1087.77	950.69	790.12	587.10	254.96
IGA-FSDT[b]	21 726	1087.77	947.28	781.93	570.51	198.87
IGA-IHTSDT[a]	21 915	1079.22	941.19	779.01	572.52	220.53
IGA-IHTSDT[b]	21 360	1079.22	937.26	769.53	553.08	140.04
IGA-IHSDT[a]	22 057	1081.51	944.14	782.97	578.44	236.77
IGA-IHSDT[b]	21 427	1081.51	939.73	772.38	556.69	152.65

[a]Present von Kármán solution.
[b]Present Green–Lagrange solution.

value of T_* is taken as 21 000 K, which has been chosen as a lower value than the lowest critical buckling temperature $(T_\lambda = 21360\,\mathrm{K})$ as shown in Table 17 to safeguard the buckled state. Where critical buckling temperature (T_λ) is obtained by solving $(\boldsymbol{K}_l - (-T_\lambda \boldsymbol{K}_g))\,\boldsymbol{q}^d = 0$. From this example, we can emphasize the use of Green–Lagrange for the moderately thick/thick plate when subjected to temperature beyond one-fourth of the critical buckling temperature.

4.4.5. Forced vibration analysis of cross-ply laminated plate with temperature and moisture dependent material properties

After establishing the efficiency of present IGA-NPSDT model for free vibration analysis, now the applicability of the present model is extended for transient analysis. For this, a twenty-layered simply supported ($SSSS1$) cross-ply $(0°/90°)_{10}$ laminated plate initially under uniform thermal environment ($\Delta T = T - 300 =$ constant) has been considered for the transient analysis. The plate after attaining the static equilibrium is then subjected to uniform transverse step loading of magnitude $P = 100$ N/m^2 for time $t_1 = 0.03$ s. The laminated composite plate is made up of material MM6 [26,61] listed in Table 1 with side-length, $a = b = 0.5$ m and thickness, $h = 5$ mm.

In Fig. 6, the transient response of the central deflection with respect to reference temperature $T = 300$ K and elevated temperature 400 K and 425 K is shown. It can be observed from the Fig. 6 that the results obtained from the present investigation are in well agreement with the available results of Parhi et al. [26] by FEM-FSDT. Based on the results shown in the Fig. 6, one can conclude that as temperature increases, stiffness decreases which in turn increase the central deflection and decrease the frequency with respect to reference transient response. Here, the same time step $\Delta t = 10^{-6}$ s is considered as taken in Ref. [26].

Further, the same problem is analyzed for the $C = 0\%$, 1% and 1.5% moisture concentration and the obtained response is presented in Fig. 7. The present IGA-IHTSDT results are compared with the available solution [26] and found to be in well agreement. Also, with increase in moisture concentration, stiffness decreases therefore central deflection increases and frequency decreases. In accordance with examples shown in free vibration for thin plate, here also exact same response is observed for both von Kármán and Green–Lagrange nonlinearity in stress geometric stiffness matrix for both IGA-IHTSDT and IGA-IHSDT model due to the consideration of thin plate, $a/h = 100$. Therefore, only Green–Lagrange nonlinearity solution has been shown Fig. 7.

4.4.6. Forced vibration analysis of simply supported cross-ply laminated plate under uniform thermal load

In order to further verify the accuracy of present IGA-NPSDT model for moderately thick plate, a simply supported ($SSSS2$) three-layered $(0°/90°/0°)$ cross-ply laminated composite plate initially under uniform thermal environment (ΔT) is considered for the transient analysis. The laminated composite plate consists of length $a = b = 10h$ and thickness $h = 2$ in. The material properties used for this analysis are MM9 [62], given in Table 1. This sample examples is solved by Shen [62] using state variable approach by considering TSDT and von Kármán nonlinearity.

Further, after attaining the static equilibrium of the plate, a sinusoidal transverse step loading, $P = P_w \sin\left(\frac{x\pi}{a}\right)\sin\left(\frac{y\pi}{b}\right)$ with magnitude $P_w = 5000$ psi is applied on the top surface of the plate for time $t_1 = 0.003$ s with time step, $\Delta t = 10^{-6}$ s. The transient response of the central deflection for the uniform temperature change, $\Delta T = 200$ K and 400 K is presented in Fig. 8a along with response in reference condition, $\Delta T = 0$ K. From Fig. 8a, it is observed that the present IGA-IHTSDT results are in close resemblance with the available solution [62] using TSDT. The accuracy of HSDT and TSDT are observed to be almost same. A little higher transient deflection amplitude with lower frequency is observed in the present IGA-IHTSDT due to consideration of Green–Lagrange nonlinearity. Hence, with this problem the applicability and efficacy of present IGA-NPSDT model is validated for dynamic response of initially stresses laminated composite plate.

Apart from this, the fast Fourier transform (FFT) approach is employed to obtain the frequency domain response from the time-domain solution mentioned in Fig. 8a. The FFT solution presented in Fig. 8b also marked the natural frequency obtained from this approach. It provides a unique technique to obtain the natural frequency from the undamped transient response. This method may have practical implication in structural analysis as the transient response is often measured easily.

Now a damped transient response is obtained for the same problem mentioned above. The Rayleigh damping model is employed with damping ratios of $\xi = 1\%$, 2%, and 3%. The obtained transient damped

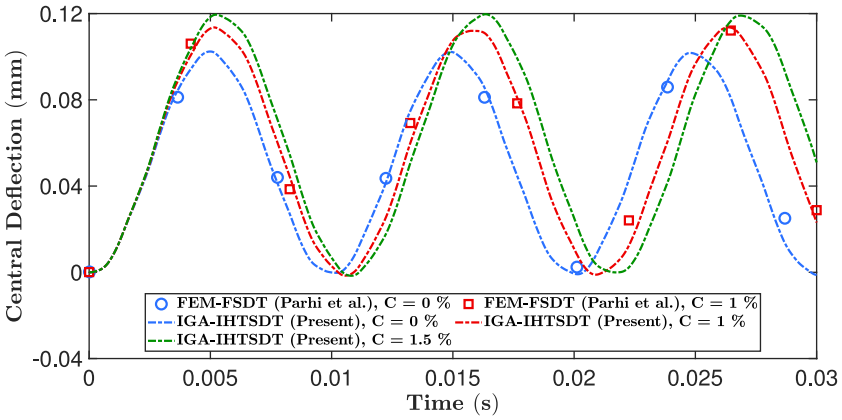

Fig. 7. Central deflection of twenty-layered cross-ply laminate $(0°/90°)_{10}$ plate subjected to uniformly distributed step loading with uniform moisture concentration under simply supported ($SSSS1$) boundary condition for moisture concentration, $C = 0\%$, 1% and 1.5%.

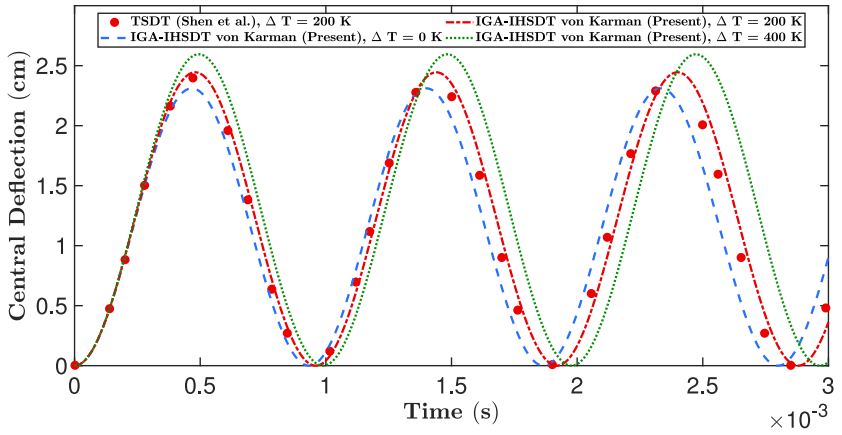

(a) Time domain representation.

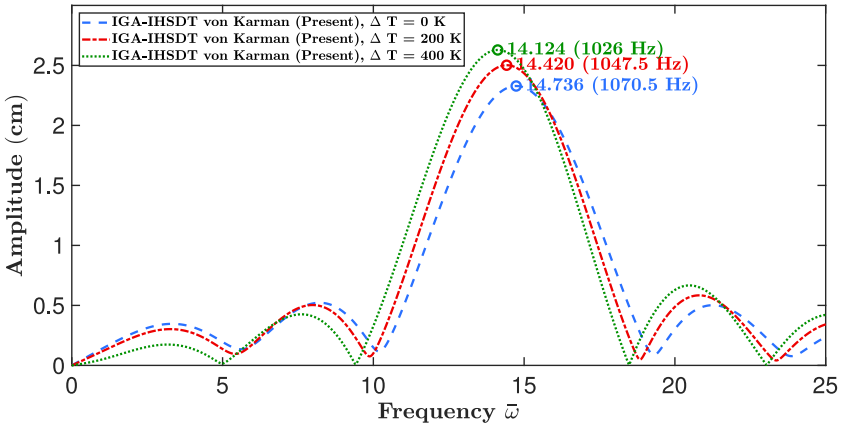

(b) Frequency domain representation.

Fig. 8. Time–history response and its Fourier transform of central deflection of simply supported ($SSSS2$) three-layered cross-ply $(0°/90°/0°)$ laminated composite plate under uniform thermal environment ($\Delta T = 200$ K and 400 K) subjected to sinusoidal step loading.

solution is shown in Fig. 9a. Further, the FFT response has also been obtained and shown in Fig. 9b. In this case also, the natural frequency has been marked in the plot which provides the natural frequency obtained from damped transient response. Again the method employed here to calculate the natural frequency is important. As in the practical sense, every forced vibration response has inherent damping characteristics and therefore this approach would be appropriate for analyzing such problem for the calculation of natural frequency.

4.4.7. Harmonic analysis of simply supported cross-ply laminated plate under uniform thermal load

To provide a complete view of the dynamic analysis, a steady-state problem with all the specification mentioned in previous problem is considered for harmonic analysis. To obtained the harmonic analysis under the thermal environment, a three-layered cross-ply $(0°/90°/0°)$ laminated composite plate having material properties MM9 [62] is considered. A transverse harmonic force, $P = P_0 cos(\omega t)$, with sinusoidal distributed load (SSL) having magnitude, $P_0 = 1\,\mathrm{N/m^2}$, is applied to the

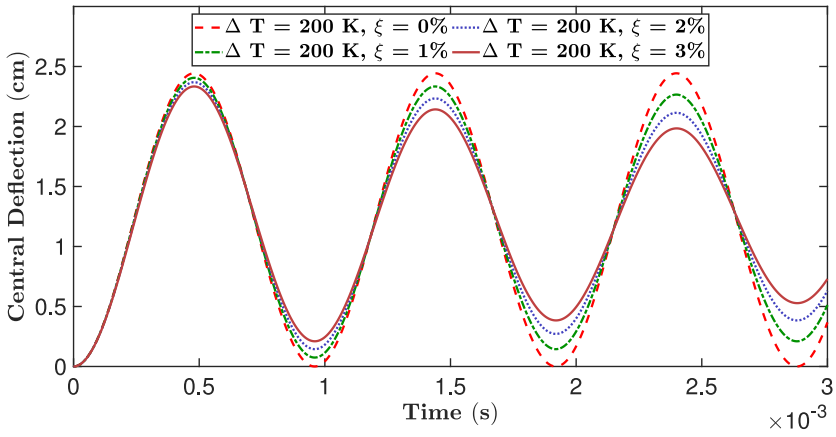

(a) Time domain representation.

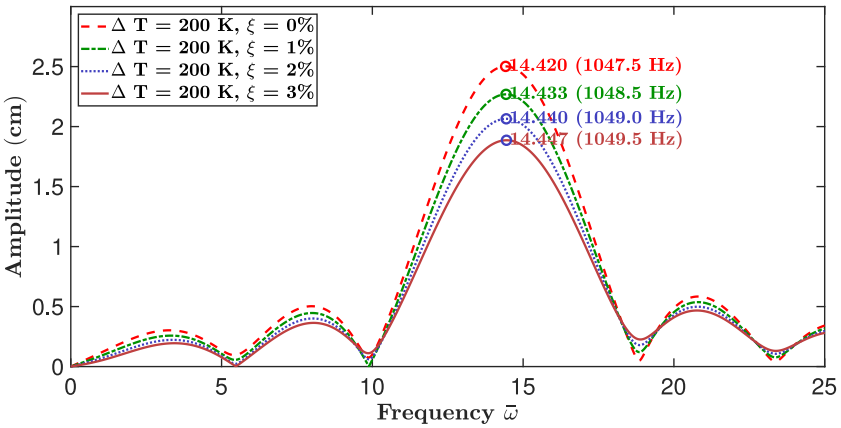

(b) Frequency domain representation.

Fig. 9. Time–history response with damping and its Fourier transform of central deflection of simply supported ($SSSS2$) three-layered cross-ply ($0°/90°/0°$) laminated composite plate under uniform thermal environment ($\Delta T = 200$ K) subjected to sinusoidal step loading.

plate. The obtained harmonic response for the uniformly distributed temperature change, $\Delta T = 200$ K is shown in Fig. 10. In this case also, the Rayleigh damped model is employed and the responses are obtained for damping ratios, $\xi = 1\%, 2\%$, and 3%. It is observed from the solution that as the change in temperature increases, the natural frequency decreases, therefore the peak of the frequency response shifts leftward, i.e., the natural frequency decreases. Further, the peak amplitude is higher for elevated temperature for the same damping ratio due decrease in stiffness of the structure. It can be infer from this observation that at higher temperature, higher damping ratio is required to maintain the same depression in the response. The steady-state solution has also been obtained by ANSYS package using four noded shell element with 50 × 50 element mesh and the present IGA response is found to be in well agreement.

5. Conclusion

A computationally efficient NURBS-based isogeometric plate model incorporating nonpolynomial shear deformation theory is proposed for static and dynamic analysis of laminated and sandwich composite plate under hygrothermal environment. The analysis includes the static, damped/undamped transient response and its fast Fourier transform, and harmonic response under hygrothermal environment. Firstly, the present model is verified with high accuracy and precision against the available and obtained closed-form and 3D elasticity solutions for thermal bending analysis of cross-ply and angle-ply composite plates. Further, the importance of Green–Lagrange nonlinearity over von Kármán for modeling the geometric stiffness matrix to incorporate stress stiffening is also highlighted.

The obtained transient damped/undamped solutions and their FFT responses conclude that the present FFT approach would be appropriate for calculating natural frequency from transient response. Harmonic response demonstrates that at higher temperature, higher damping ratio is required to maintain the same depression in the response. The present work shows a clear demonstration of the high accuracy, reliability and applicability of IGA-NPSDT model for static and dynamic analysis through rigorous illustration of varieties of examples. Furthermore, it is noticed that the accuracy of IGA-NPSDT is highly dependent upon the theory used for the analysis, i.e., IHSDT and IHTSDT. Particularly, the accuracy of IHTSDT is found to be almost same as that of TSDT which is polynomial shear deformation theory. Moreover, it is observed that the theory which predicts the static solution in better way, will not be necessarily predicting the dynamic solution with the same accuracy. Moreover, due to high inter-element continuity possessed by NURBS basis function, the present formulation reduces the computational cost and hence, increases the computational efficiency.

Thus, these findings fulfill the available gap for the accurate and efficient solution in the literature through the development of IGA-NPSDT model. The approach used in the present analysis is of great interest for the computationally efficient modeling of structures under hygrothermal environment. Apart from that, the findings of the present work is useful for the design and analysis of multilayered composite

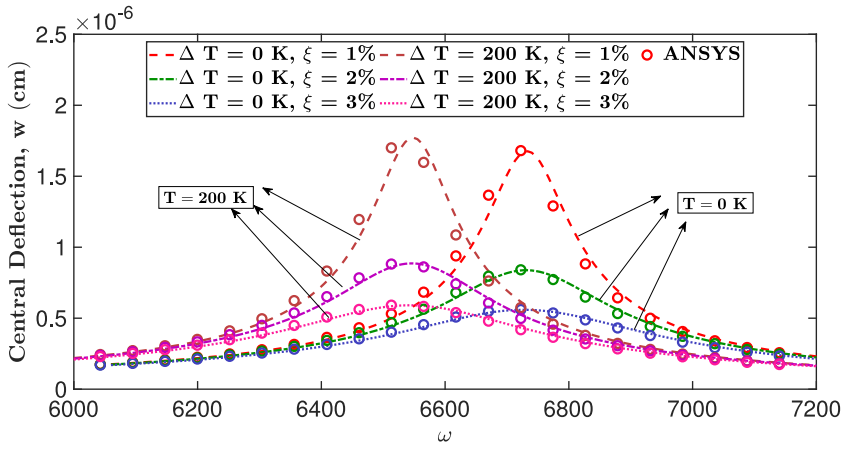

Fig. 10. Steady-state response of three-layered cross-ply laminated (0°/90°/0°) plate subjected to sinusoidally load (SSL) under simply supported (*S.S.S.S*2) boundary condition for temperature, $\Delta T = 0$ K and 200 K.

$$\mathbb{N}_b = \begin{bmatrix}
N_{xx} & N_{xy} & 0 & 0 & 0 & 0 & -M_{xx} & -M_{xy} & 0 & 0 & P_{xx} & P_{xy} & 0 & 0 \\
N_{xy} & N_{yy} & 0 & 0 & 0 & 0 & -M_{xy} & -M_{yy} & 0 & 0 & P_{xy} & P_{yy} & 0 & 0 \\
0 & 0 & N_{xx} & N_{xy} & 0 & 0 & 0 & 0 & -M_{xx} & -M_{xy} & 0 & 0 & P_{xx} & P_{xy} \\
0 & 0 & N_{xy} & N_{yy} & 0 & 0 & 0 & 0 & -M_{xy} & -M_{yy} & 0 & 0 & P_{xy} & P_{yy} \\
0 & 0 & 0 & 0 & N_{xx} & N_{xy} & 0 & 0 & 0 & 0 & 0 & 0 & 0 & 0 \\
0 & 0 & 0 & 0 & N_{xy} & N_{yy} & 0 & 0 & 0 & 0 & 0 & 0 & 0 & 0 \\
-M_{xx} & -M_{xy} & 0 & 0 & 0 & 0 & Q_{xx} & Q_{xy} & 0 & 0 & -R_{xx} & -R_{xy} & 0 & 0 \\
-M_{xy} & -M_{yy} & 0 & 0 & 0 & 0 & Q_{xy} & Q_{yy} & 0 & 0 & -R_{xy} & -R_{yy} & 0 & 0 \\
0 & 0 & -M_{xx} & -M_{xy} & 0 & 0 & 0 & 0 & Q_{xx} & Q_{xy} & 0 & 0 & -R_{xx} & -R_{xy} \\
0 & 0 & -M_{xy} & -M_{yy} & 0 & 0 & 0 & 0 & Q_{xy} & Q_{yy} & 0 & 0 & -R_{xy} & -R_{yy} \\
P_{xx} & P_{xy} & 0 & 0 & 0 & 0 & -R_{xx} & -R_{xy} & 0 & 0 & S_{xx} & S_{xy} & 0 & 0 \\
P_{xy} & P_{yy} & 0 & 0 & 0 & 0 & -R_{xy} & -R_{yy} & 0 & 0 & S_{xy} & S_{yy} & 0 & 0 \\
0 & 0 & 0 & 0 & 0 & 0 & 0 & 0 & -R_{xx} & -R_{xy} & 0 & 0 & S_{xx} & S_{xy} \\
0 & 0 & 0 & 0 & 0 & 0 & 0 & 0 & -R_{xy} & -R_{yy} & 0 & 0 & S_{xy} & S_{yy}
\end{bmatrix} \tag{A.1}$$

Box VI.

structures from various structural perspective as it gives a holistic understanding of static and dynamic analysis of multilayered composite plate.

CRediT authorship contribution statement

Abha Gupta: Conceptualization, Methodology, Data curation, Visualization, Writing – original draft, Programming. **Surendra Verma:** Conceptualization, Methodology, Visualization, Writing – original draft, Programming. **Anup Ghosh:** Conceptualization, Supervision, Reviewing and editing.

Declaration of competing interest

The authors declare that they have no known competing financial interests or personal relationships that could have appeared to influence the work reported in this paper.

Appendix A

See Eqs. (A.1) and (A.2) are given as in Boxes VI and VII.

Appendix B. Navier solution for simply supported anti-symmetric cross-ply composite plate under thermal load, ΔT (z)

$$u_0 = \sum_{m=1}^{\infty}\sum_{n=1}^{\infty} U_{mn} cos(\alpha x)\, sin(\beta y) \qquad v_0 = \sum_{m=1}^{\infty}\sum_{n=1}^{\infty} V_{mn} sin(\alpha x)\, cos(\beta y)$$

$$w_0 = \sum_{m=1}^{\infty}\sum_{n=1}^{\infty} W_{mn} sin(\alpha x)\, sin(\beta y) \qquad \theta_x = \sum_{m=1}^{\infty}\sum_{n=1}^{\infty} X_{mn} cos(\alpha x)\, sin(\beta y)$$

$$\theta_y = \sum_{m=1}^{\infty}\sum_{n=1}^{\infty} Y_{mn} sin(\alpha x)\, cos(\beta y)$$

$$\begin{bmatrix}
K_{11} & K_{12} & K_{13} & K_{14} & K_{15} \\
 & K_{22} & K_{23} & K_{24} & K_{25} \\
 & & K_{33} & K_{34} & K_{35} \\
 & \text{sym} & & K_{44} & K_{45} \\
 & & & & K_{55}
\end{bmatrix}
\begin{Bmatrix} U_{mn} \\ V_{mn} \\ W_{mn} \\ X_{mn} \\ Y_{mn} \end{Bmatrix}$$

$$= \begin{Bmatrix} 0 \\ 0 \\ F_{mn} \\ 0 \\ 0 \end{Bmatrix} - \begin{Bmatrix} \alpha N^{xx}_{mn} \\ \beta F^{yy}_{mn} \\ -\alpha^2 M^{xx}_{mn} - \beta^2 M^{yy}_{mn} \\ \alpha P^{xx}_{mn} \\ \beta P^{yy}_{mn} \end{Bmatrix}$$

$$\mathbb{N}_s = \begin{bmatrix}
0 & 0 & 0 & 0 & -N_{xz} & -N_{yz} & 0 & 0 & M_{xz} & M_{yz} & 0 & 0 & -P_{xz} & -P_{yz} & 0 & 0 \\
0 & 0 & 0 & 0 & 0 & 0 & -N_{xz} & -N_{yz} & 0 & 0 & M_{xz} & M_{yz} & 0 & 0 & -P_{xz} & -P_{yz} \\
0 & 0 & 0 & 0 & Q_{xz} & Q_{yz} & 0 & 0 & -R_{xz} & -R_{yz} & 0 & 0 & S_{xz} & S_{yz} & 0 & 0 \\
0 & 0 & 0 & 0 & 0 & 0 & Q_{xz} & Q_{yz} & 0 & 0 & -R_{xz} & -R_{yz} & 0 & 0 & S_{xz} & S_{yz} \\
-N_{xz} & 0 & Q_{xz} & 0 & 0 & 0 & 0 & 0 & 0 & 0 & 0 & 0 & 0 & 0 & 0 & 0 \\
-N_{yz} & 0 & Q_{yz} & 0 & 0 & 0 & 0 & 0 & 0 & 0 & 0 & 0 & 0 & 0 & 0 & 0 \\
0 & -N_{xz} & 0 & Q_{xz} & 0 & 0 & 0 & 0 & 0 & 0 & 0 & 0 & 0 & 0 & 0 & 0 \\
0 & -N_{yz} & 0 & Q_{yz} & 0 & 0 & 0 & 0 & 0 & 0 & 0 & 0 & 0 & 0 & 0 & 0 \\
M_{xz} & 0 & -R_{xz} & 0 & 0 & 0 & 0 & 0 & 0 & 0 & 0 & 0 & 0 & 0 & 0 & 0 \\
M_{yz} & 0 & -R_{yz} & 0 & 0 & 0 & 0 & 0 & 0 & 0 & 0 & 0 & 0 & 0 & 0 & 0 \\
0 & M_{xz} & 0 & -R_{xz} & 0 & 0 & 0 & 0 & 0 & 0 & 0 & 0 & 0 & 0 & 0 & 0 \\
0 & M_{yz} & 0 & -R_{yz} & 0 & 0 & 0 & 0 & 0 & 0 & 0 & 0 & 0 & 0 & 0 & 0 \\
-P_{xz} & 0 & S_{xz} & 0 & 0 & 0 & 0 & 0 & 0 & 0 & 0 & 0 & 0 & 0 & 0 & 0 \\
-P_{yz} & 0 & S_{yz} & 0 & 0 & 0 & 0 & 0 & 0 & 0 & 0 & 0 & 0 & 0 & 0 & 0 \\
0 & -P_{xz} & 0 & S_{xz} & 0 & 0 & 0 & 0 & 0 & 0 & 0 & 0 & 0 & 0 & 0 & 0 \\
0 & -P_{yz} & 0 & S_{yz} & 0 & 0 & 0 & 0 & 0 & 0 & 0 & 0 & 0 & 0 & 0 & 0
\end{bmatrix} \tag{A.2}$$

Box VII.

$$K_{11} = \alpha^2 A_{11} + \beta^2 A_{66} \qquad K_{12} = \alpha\beta A_{12} + \alpha\beta A_{66}$$
$$K_{13} = -\alpha\left(\alpha^2 B_{11} + \beta^2 B_{12} + 2\beta^2 B_{66}\right) \qquad K_{14} = \alpha^2 C_{11} + \beta^2 C_{66}$$
$$K_{15} = \alpha\beta C_{12} + \alpha\beta C_{66} \qquad K_{22} = \alpha^2 A_{66} + \beta^2 A_{22}$$
$$K_{23} = -\beta\left(\alpha^2 B_{12} + \beta^2 B_{22} + 2\alpha^2 B_{66}\right) \qquad K_{24} = \alpha\beta C_{12} + \alpha\beta C_{66}$$
$$K_{25} = \alpha^2 C_{66} + \beta^2 C_{22} \qquad K_{33} = \alpha^4 D_{11} + 2\alpha^2\beta^2 D_{12} + \beta^4 D_{22} + 4\alpha^2\beta^2 D_{66}$$
$$K_{34} = -\alpha\left(\alpha^2 E_{11} + \beta^2 E_{12} + 2\beta^2 E_{66}\right) \qquad K_{35} = -\beta\left(\alpha^2 E_{12} + \beta^2 E_{22} + 2\alpha^2 E_{66}\right)$$
$$K_{44} = A_{55} + \alpha^2 F_{11} + \beta^2 F_{66} \qquad K_{45} = \alpha\beta F_{12} + \alpha\beta F_{66}$$
$$K_{55} = A_{44} + \alpha^2 F_{66} + \beta^2 F_{22}$$
$$F_{mn} = \begin{cases} P_0 & \text{Spartially Sinusoidal Mechanical load} \\ 16P_0/\pi^2 mn & \text{Spartially Uniform Mechanical load} \end{cases}$$
$$\Delta T_{mn} = \begin{cases} \Delta T(z) & \text{Spartially Sinusoidal Temperature} \\ 16\Delta T(z)/\pi^2 mn & \text{Spartially Uniform Temperature} \end{cases}$$
$$N_{mn} = \int_{-h/2}^{h/2} \bar{Q}\boldsymbol{\alpha}\Delta T_{mn}(z)\,dz \qquad M_{mn} = \int_{-h/2}^{h/2} \bar{Q}\boldsymbol{\alpha} z\Delta T_{mn}(z)$$
$$P_{mn} = \int_{-h/2}^{h/2} \bar{Q}\boldsymbol{\alpha} f(z)\,\Delta T_{mn}(z)\,dz$$
$$\left[A_{ij}\right] = \int_{-h/2}^{h/2} f'(z)\,\bar{Q}_{ij}\,dz \qquad i,j = 4,5$$
$$\left[A_{ij}\right] = \int_{-h/2}^{h/2} \bar{Q}_{ij}\,dz \qquad \left[B_{ij}\right] = \int_{-h/2}^{h/2} z\bar{Q}_{ij}\,dz$$
$$\left[C_{ij}\right] = \int_{-h/2}^{h/2} f(z)\,\bar{Q}_{ij}\,dz$$
$$\left[D_{ij}\right] = \int_{-h/2}^{h/2} G(z)\,\bar{Q}_{ij}\,dz \qquad \left[E_{ij}\right] = \int_{-h/2}^{h/2} z^2\bar{Q}_{ij}\,dz$$
$$\left[F_{ij}\right] = \int_{-h/2}^{h/2} zf(z)\,\bar{Q}_{ij}\,dz$$
$$i,j = 1,2,6$$

For sinusoidal distribution, Navier solution converged with one term only, i.e., $m, n = 1$. On the other hand, solution for uniform distribution requires $m, n = 1, 3, 5....$

References

[1] Abrate S, Sciuva MD. Equivalent single layer theories for composite and sandwich structures: A review. Compos Struct 2017;179:482–94. http://dx.doi.org/10.1016/j.compstruct.2017.07.090.

[2] Pai PF. A new look at shear correction factors and warping functions of anisotropic laminates. Int J Solids Struct 1995;32(16):2295–313. http://dx.doi.org/10.1016/0020-7683(94)00258-x.

[3] Gupta A, Ghosh A. Static and transient analysis of sandwich composite plates using isogeometric analysis. Mech Adv Mater Struct 2018;1–7.

[4] Reddy JN. A simple higher-order theory for laminated composite plates. J Appl Mech 1984;51(4):745–52. http://dx.doi.org/10.1115/1.3167719.

[5] Sayyad AS, Ghugal YM. On the free vibration analysis of laminated composite and sandwich plates: A review of recent literature with some numerical results. Compos Struct 2015;129:177–201. http://dx.doi.org/10.1016/j.compstruct.2015.04.007.

[6] Thakur BR, Verma S, Singh B, Maiti D. Geometrically nonlinear dynamic analysis of laminated composite plate using a nonpolynomial shear deformation theory. Int J Non-Linear Mech 2021;128:103635. http://dx.doi.org/10.1016/j.ijnonlinmec.2020.103635.

[7] Verma S, Thakur BR, Singh B, Maiti D. Geometrically nonlinear flexural analysis of multilayered composite plate using polynomial and non-polynomial shear deformation theories. Aerosp Sci Technol 2021;112:106635. http://dx.doi.org/10.1016/j.ast.2021.106635.

[8] Thakur BR, Verma S, Singh B, Maiti D. Dynamic analysis of folded laminated composite plate using nonpolynomial shear deformation theory. Aerosp Sci Technol 2020;106:106083. http://dx.doi.org/10.1016/j.ast.2020.106083.

[9] Cottrell JA, Hughes TJ, Bazilevs Y. Isogeometric analysis: Toward integration of CAD and FEA. New York, USA: John Wiley & Sons; 2009.

[10] Gupta A, Ghosh A. Isogeometric static and dynamic analysis of laminated and sandwich composite plates using nonpolynomial shear deformation theory. Composites B 2019;176:107295. http://dx.doi.org/10.1016/j.compositesb.2019.107295.

[11] Hughes T, Cottrell J, Bazilevs Y. Isogeometric analysis: CAD, finite elements, NURBS, exact geometry and mesh refinement. Comput Methods Appl Mech Engrg 2005;194(39–41):4135–95. http://dx.doi.org/10.1016/j.cma.2004.10.008.

[12] Bazilevs Y, da Veiga LB, Cottrell JA, Hughes TJR, Sangalli G. Isogeometric analysis: Approximation, stability and error estimates for h-refined meshes. Math Models Methods Appl Sci 2006;16(07):1031–90. http://dx.doi.org/10.1142/s0218202506001455.

[13] Cottrell J, Reali A, Bazilevs Y, Hughes T. Isogeometric analysis of structural vibrations. Comput Methods Appl Mech Engrg 2006;195(41–43):5257–96. http://dx.doi.org/10.1016/j.cma.2005.09.027.

[14] Do H, Tan YY, Ramos N, Kiendl J, Weeger O. Nonlinear isogeometric multiscale simulation for design and fabrication of functionally graded knitted textiles. Composites B 2020;202:108416. http://dx.doi.org/10.1016/j.compositesb.2020.108416.

[15] Thakur BR, Verma S, Singh BN, Maiti D. Dynamic analysis of flat and folded laminated composite plates under hygrothermal environment using a nonpolynomial shear deformation theory. Compos Struct 2021;114327. http://dx.doi.org/10.1016/j.compstruct.2021.114327.

[16] Garg A, Chalak H. A review on analysis of laminated composite and sandwich structures under hygrothermal conditions. Thin-Walled Struct 2019;142:205–26. http://dx.doi.org/10.1016/j.tws.2019.05.005.

[17] Zhong Y, Cheng M, Zhang X, Hu H, Cao D, Li S. Hygrothermal durability of glass and carbon fiber reinforced composites – A comparative study. Compos Struct 2019;211:134–43. http://dx.doi.org/10.1016/j.compstruct.2018.12.034.

[18] Ram KS, Sinha P. Hygrothermal effects on the bending characteristics of laminated composite plates. Comput Struct 1991;40(4):1009–15. http://dx.doi.org/10.1016/0045-7949(91)90332-g.

[19] Patel B, Ganapathi M, Makhecha D. Hygrothermal effects on the structural behaviour of thick composite laminates using higher-order theory. Compos Struct 2002;56(1):25–34. http://dx.doi.org/10.1016/s0263-8223(01)00182-9.

[20] Zenkour AM. Hygrothermal effects on the bending of angle-ply composite plates using a sinusoidal theory. Compos Struct 2012;94(12):3685–96. http://dx.doi.org/10.1016/j.compstruct.2012.05.033.

[21] Joshan Y, Grover N, Singh B. Analytical modelling for thermo-mechanical analysis of cross-ply and angle-ply laminated composite plates. Aerosp Sci Technol 2017;70:137–51. http://dx.doi.org/10.1016/j.ast.2017.07.041.

[22] Moleiro F, Soares CM, Carrera E. Three-dimensional exact hygro-thermo-elastic solutions for multilayered plates: Composite laminates, fibre metal laminates and sandwich plates. Compos Struct 2019;216:260–78. http://dx.doi.org/10.1016/j.compstruct.2019.02.071.

[23] Han J-W, Kim J-S, Cho M. New enhanced first-order shear deformation theory for thermo-mechanical analysis of laminated composite and sandwich plates. Composites B 2017;116:422–50. http://dx.doi.org/10.1016/j.compositesb.2016.10.087.

[24] Murugesan N, Rajamohan V. Interlaminar shear stresses in laminated composite plates under thermal and mechanical loading. Mech Adv Mater Struct 2015;23(5):554–64. http://dx.doi.org/10.1080/15376494.2015.1007190.

[25] Ram KS, Sinha P. Hygrothermal effects on the free vibration of laminated composite plates. J Sound Vib 1992;158(1):133–48. http://dx.doi.org/10.1016/0022-460x(92)90669-o.

[26] Parhi P, Bhattacharyya S, Sinha P. Hygrothermal effects on the dynamic behavior of multiple delaminated composite plates and shells. J Sound Vib 2001;248(2):195–214. http://dx.doi.org/10.1006/jsvi.2000.3506.

[27] Naidu NS, Sinha P. Nonlinear transient analysis of laminated composite shells in hygrothermal environments. Compos Struct 2006;72(3):280–8. http://dx.doi.org/10.1016/j.compstruct.2004.12.001.

[28] Li W, Li Y. Vibration and sound radiation of an asymmetric laminated plate in thermal environments. Acta Mech Solida Sin 2015;28(1):11–22. http://dx.doi.org/10.1016/s0894-9166(15)60011-8.

[29] Panda H, Sahu S, Parhi P. Hygrothermal effects on free vibration of delaminated woven fiber composite plates – Numerical and experimental results. Compos Struct 2013;96:502–13. http://dx.doi.org/10.1016/j.compstruct.2012.08.057.

[30] Makhecha D, Ganapathi M, Patel B. Dynamic analysis of laminated composite plates subjected to thermal/mechanical loads using an accurate theory. Compos Struct 2001;51(3):221–36. http://dx.doi.org/10.1016/s0263-8223(00)00133-1.

[31] Matsunaga H. Free vibration and stability of angle-ply laminated composite and sandwich plates under thermal loading. Compos Struct 2007;77(2):249–62. http://dx.doi.org/10.1016/j.compstruct.2005.07.002.

[32] Bouazza M, Zenkour AM. Free vibration characteristics of multilayered composite plates in a hygrothermal environment via the refined hyperbolic theory. Eur Phys J Plus 2018;133(6). http://dx.doi.org/10.1140/epjp/i2018-12050-x.

[33] Vinyas M, Kattimani S. Finite element evaluation of free vibration characteristics of magneto-electro-elastic rectangular plates in hygrothermal environment using higher-order shear deformation theory. Compos Struct 2018;202:1339–52. http://dx.doi.org/10.1016/j.compstruct.2018.06.069.

[34] Patton A, Antolín P, Dufour J-E, Kiendl J, Reali A. Accurate equilibrium-based interlaminar stress recovery for isogeometric laminated composite Kirchhoff plates. Compos Struct 2021;256:112976. http://dx.doi.org/10.1016/j.compstruct.2020.112976.

[35] Zhong S, Jin G, Ye T, Zhang J, Xue Y, Chen M. Isogeometric vibration analysis of multi-directional functionally gradient circular, elliptical and sector plates with variable thickness. Compos Struct 2020;250:112470. http://dx.doi.org/10.1016/j.compstruct.2020.112470.

[36] Hasim K, Kefal A. Isogeometric static analysis of laminated plates with curvilinear fibers based on Refined Zigzag Theory. Compos Struct 2021;256:113097. http://dx.doi.org/10.1016/j.compstruct.2020.113097.

[37] Patton A, Dufour J-E, Antolin P, Reali A. Fast and accurate elastic analysis of laminated composite plates via isogeometric collocation and an equilibrium-based stress recovery approach. Compos Struct 2019;225:111026. http://dx.doi.org/10.1016/j.compstruct.2019.111026.

[38] Kiendl J, Bazilevs Y, Hsu M-C, Wüchner R, Bletzinger K-U. The bending strip method for isogeometric analysis of Kirchhoff–Love shell structures comprised of multiple patches. Comput Methods Appl Mech Engrg 2010;199(37–40):2403–16. http://dx.doi.org/10.1016/j.cma.2010.03.029.

[39] Fazilati J, Khalafi V. Dynamic analysis of the composite laminated repaired perforated plates by using multi-patch IGA method. Chin J Aeronaut 2021;34(1):266–80. http://dx.doi.org/10.1016/j.cja.2020.09.038.

[40] Shafei E, Faroughi S, Rabczuk T. Multi-patch NURBS formulation for anisotropic variable angle tow composite plates. Compos Struct 2020;241:111964. http://dx.doi.org/10.1016/j.compstruct.2020.111964.

[41] Obohat MA, Tahvilian E, Yildizdag ME, Ergin A. Three-dimensional multi-patch isogeometric analysis of composite laminates with a discontinuous Galerkin approach. Proc Inst Mech Eng M 2020;147509022092573. http://dx.doi.org/10.1177/1475090220925734.

[42] Yildizdag ME, Demirtas M, Ergin A. Multipatch discontinuous Galerkin isogeometric analysis of composite laminates. Contin Mech Thermodyn 2018;32(3):607–20. http://dx.doi.org/10.1007/s00161-018-0696-9.

[43] Tran LV, Wahab MA, Kim S-E. An isogeometric finite element approach for thermal bending and buckling analyses of laminated composite plates. Compos Struct 2017;179:35–49. http://dx.doi.org/10.1016/j.compstruct.2017.07.056.

[44] Gupta A, Ghosh A. NURBS-based thermo-elastic analyses of laminated and sandwich composite plates. Sādhanā 2019;44(4). http://dx.doi.org/10.1007/s12046-019-1063-7.

[45] Phung-Van P, Tran LV, Ferreira AJM, Nguyen-Xuan H, Abdel-Wahab M. Nonlinear transient isogeometric analysis of smart piezoelectric functionally graded material plates based on generalized shear deformation theory under thermo-electro-mechanical loads. Nonlinear Dynam 2016;87(2):879–94. http://dx.doi.org/10.1007/s11071-016-3085-6.

[46] Phung-Van P, Thai CH, Nguyen-Xuan H, Wahab MA. Porosity-dependent nonlinear transient responses of functionally graded nanoplates using isogeometric analysis. Composites B 2019;164:215–25. http://dx.doi.org/10.1016/j.compositesb.2018.11.036.

[47] Nguyen HX, Nguyen TN, Abdel-Wahab M, Bordas S, Nguyen-Xuan H, Vo TP. A refined quasi-3D isogeometric analysis for functionally graded microplates based on the modified couple stress theory. Comput Methods Appl Mech Engrg 2017;313:904–40. http://dx.doi.org/10.1016/j.cma.2016.10.002.

[48] Cuong-Le T, Nguyen KD, Nguyen-Trong N, Khatir S, Nguyen-Xuan H, Abdel-Wahab M. A three-dimensional solution for free vibration and buckling of annular plate, conical, cylinder and cylindrical shell of FG porous-cellular materials using IGA. Compos Struct 2021;259:113216. http://dx.doi.org/10.1016/j.compstruct.2020.113216.

[49] Shi P, Dong C, Sun F, Liu W, Hu Q. A new higher order shear deformation theory for static, vibration and buckling responses of laminated plates with the isogeometric analysis. Compos Struct 2018;204:342–58. http://dx.doi.org/10.1016/j.compstruct.2018.07.080.

[50] Rogers D. An introduction to NURBS: With historical perspective. San Diego, CA: Academic Press; 2001.

[51] Bhimaraddi A. Buckling and post-buckling behavior of laminated plates using the generalized nonlinear formulation. Int J Mech Sci 1992;34(9):703–15. http://dx.doi.org/10.1016/0020-7403(92)90003-y.

[52] Tran LV, Lee J, Nguyen-Van H, Nguyen-Xuan H, Wahab MA. Geometrically nonlinear isogeometric analysis of laminated composite plates based on higher-order shear deformation theory. Int J Non-Linear Mech 2015;72:42–52. http://dx.doi.org/10.1016/j.ijnonlinmec.2015.02.007.

[53] Joshan Y, Grover N, Singh B. A new non-polynomial four variable shear deformation theory in axiomatic formulation for hygro-thermo-mechanical analysis of laminated composite plates. Compos Struct 2017;182:685–93. http://dx.doi.org/10.1016/j.compstruct.2017.09.029.

[54] Reddy JN. Mechanics of laminated composite plates and shells: Theory and analysis. 2nd ed.. Boca Raton, USA: CRC Press; 2004.

[55] Naidu NS, Sinha P. Nonlinear free vibration analysis of laminated composite shells in hygrothermal environments. Compos Struct 2007;77(4):475–83. http://dx.doi.org/10.1016/j.compstruct.2005.08.002.

[56] Nguyen VP, Bordas S. Extended isogeometric analysis for strong and weak discontinuities. In: Isogeometric methods for numerical simulation. Springer Vienna; 2015, p. 21–120. http://dx.doi.org/10.1007/978-3-7091-1843-6_2.

[57] Reddy JN, Hsu YS. Effects of shear deformation and anisotropy on the thermal bending of layered composite plates. J Therm Stresses 1980;3(4):475–93. http://dx.doi.org/10.1080/01495738008926984.

[58] Shariyat M. A generalized global–local high-order theory for bending and vibration analyses of sandwich plates subjected to thermo-mechanical loads. Int J Mech Sci 2010;52(3):495–514. http://dx.doi.org/10.1016/j.ijmecsci.2009.11.010.

[59] Liu C-F, Huang C-H. Free vibration of composite laminated plates subjected to temperature changes. Comput Struct 1996;60(1):95–101. http://dx.doi.org/10.1016/0045-7949(95)00358-4.

[60] Li X, Yu K, Han J, Song H, Zhao R. Buckling and vibro-acoustic response of the clamped composite laminated plate in thermal environment. Int J Mech Sci 2016;119:370–82. http://dx.doi.org/10.1016/j.ijmecsci.2016.10.021.

[61] Huang X-L, Shen H-S, Zheng J-J. Nonlinear vibration and dynamic response of shear deformable laminated plates in hygrothermal environments. Compos Sci Technol 2004;64(10–11):1419–35. http://dx.doi.org/10.1016/j.compscitech.2003.09.028.

[62] Shen H-S, Zheng J-J, Huang X-L. Dynamic response of shear deformable laminated plates under thermomechanical loading and resting on elastic foundations. Compos Struct 2003;60(1):57–66. http://dx.doi.org/10.1016/s0263-8223(02)00295-7.

[63] Bhimaraddi A, Chandrashekhara K. Nonlinear vibrations of heated antisymmetric angle-ply laminated plates. Int J Solids Struct 1993;30(9):1255–68. http://dx.doi.org/10.1016/0020-7683(93)90015-y.

[64] Chandrashekhara K, Tenneti R. Non-linear static and dynamic analysis of heated laminated plates: A finite element approach. Compos Sci Technol 1994;51(1):85–94. http://dx.doi.org/10.1016/0266-3538(94)90159-7.

[65] Ye J. Laminated composite plates and shells: 3D modelling. Springer Science & Business Media; 2002.

[66] Hassani B, Ganjali A, Tavakkoli M. An isogeometrical approach to error estimation and stress recovery. Eur J Mech A Solids 2012;31(1):101–9. http://dx.doi.org/10.1016/j.euromechsol.2011.08.001.

[67] Wu CH, Tauchert TR. Thermoelastic analysts of laminated plates. 2: Antisymmetric cross-ply and angle-ply laminates. J Therm Stresses 1980;3(3):365–78. http://dx.doi.org/10.1080/01495738008926975.

[68] Cetkovic M. Thermo-mechanical bending of laminated composite and sandwich plates using layerwise displacement model. Compos Struct 2015;125:388–99. http://dx.doi.org/10.1016/j.compstruct.2015.01.051.

[69] Cetkovic M. Thermo-mechanical bending of laminated composite and sandwich plates using layerwise displacement model. Compos Struct 2015;125:388–99. http://dx.doi.org/10.1016/j.compstruct.2015.01.051.

[70] Padhi A, Pandit MK. Behaviour of sandwich laminates subjected to thermal loading using higher-order zig-zag theory. J Sandw Struct Mater 2015;18(2):174–99. http://dx.doi.org/10.1177/1099636215613487.

[71] Shariyat M. A generalized global–local high-order theory for bending and vibration analyses of sandwich plates subjected to thermo-mechanical loads. Int J Mech Sci 2010;52(3):495–514. http://dx.doi.org/10.1016/j.ijmecsci.2009.11.010.

[72] Matsunaga H. A comparison between 2-D single-layer and 3-D layerwise theories for computing interlaminar stresses of laminated composite and sandwich plates subjected to thermal loadings. Compos Struct 2004;64(2):161–77. http://dx.doi.org/10.1016/j.compstruct.2003.08.001.

[73] Matsunaga H. Assessment of a global higher-order deformation theory for laminated composite and sandwich plates. Compos Struct 2002;56(3):279–91. http://dx.doi.org/10.1016/s0263-8223(02)00013-2.

[74] Zhen W, Xiaohui R. Finite element analysis of hygrothermal effects on angle-ply composite plates. J Compos Mater 2015;50(16):2215–33. http://dx.doi.org/10.1177/0021998315602944.